

RESEARCH ARTICLE

Ca²⁺ elevations disrupt interactions between intraflagellar transport and the flagella membrane in *Chlamydomonas*

Cecile Fort¹, Peter Collingridge¹, Colin Brownlee^{1,2} and Glen Wheeler^{1,*}**ABSTRACT**

The movement of ciliary membrane proteins is directed by transient interactions with intraflagellar transport (IFT) trains. The green alga *Chlamydomonas* has adapted this process for gliding motility, using retrograde IFT motors to move adhesive glycoproteins in the flagella membrane. Ca²⁺ signalling contributes directly to the gliding process, although uncertainty remains over the mechanism through which it acts. Here, we show that flagella Ca²⁺ elevations initiate the movement of paused retrograde IFT trains, which accumulate at the distal end of adherent flagella, but do not influence other IFT processes. On highly adherent surfaces, flagella exhibit high-frequency Ca²⁺ elevations that prevent the accumulation of paused retrograde IFT trains. Flagella Ca²⁺ elevations disrupt the IFT-dependent movement of microspheres along the flagella membrane, suggesting that Ca²⁺ acts by directly disrupting an interaction between retrograde IFT trains and flagella membrane glycoproteins. By regulating the extent to which glycoproteins on the flagella surface interact with IFT motor proteins on the axoneme, this signalling mechanism allows precise control of traction force and gliding motility in adherent flagella.

KEY WORDS: *Chlamydomonas*, Ca²⁺ signalling, Intraflagellar transport

INTRODUCTION

Cilia and flagella are microtubule-rich organelles that extend from the surface of many eukaryote cell types and play important roles in motility and cell signalling. The elongated morphology of cilia (length 1–20 µm and diameter of 200 nm) requires specialised mechanisms to transport proteins along its length. This is achieved through the process of intraflagellar transport (IFT), in which cargo proteins required for the assembly, maintenance and sensory functions of cilia are attached to large protein complexes (IFT particles) and moved along the axoneme through the activity of microtubule motors (Pedersen and Rosenbaum, 2008). Kinesin-2 directs movement away from the cell body (anterograde), while dynein-1b (dynein 2 in mammals) mediates the return of IFT particles towards the cell (retrograde). The anterograde IFT particles are assembled into so-called trains, which move in a processive manner to the ciliary tip. Once the anterograde IFT particles reach the ciliary tip, kinesin dissociates from the IFT particle and returns to the cell body via diffusion. The diffusive return of kinesin to the

cell body may play a critical role in regulating ciliary length, acting to limit the rate at which IFT particles can enter the flagellum (Chien et al., 2017; Hendel et al., 2018). IFT trains at the ciliary tip dissociate into multiple smaller trains and move back towards the cell body (Chien et al., 2017).

The import, export and movement of many ciliary proteins is determined by their interactions with IFT particles. IFT particles are composed of ~20 proteins arranged into two sub-complexes (IFT-A and IFT-B). Proteins within the IFT-B complex have specific roles in binding to cargo proteins, including important structural components, such as tubulin and outer arm dynein (Bhogaraju et al., 2013a; Dai et al., 2018). IFT-A proteins interact with cargo proteins involved in signalling pathways, such as G-protein-coupled receptors (Mukhopadhyay et al., 2010; Picariello et al., 2019). An additional protein complex, known as the BBsome, acts as a cargo adapter and is implicated in the transport of a range of membrane-associated ciliary proteins (Liu and Lechtreck, 2018). However, improved knowledge of the factors regulating interactions between cargo proteins and IFT particles is required to better understand the mechanisms determining the movement and distribution of ciliary proteins.

There is evidence that loading and unloading of some ciliary proteins is a highly regulated process (Lechtreck, 2015). Second messengers such as Ca²⁺ and cAMP may also contribute to the regulation of cargo binding (Mukhopadhyay et al., 2013). For example, mice lacking the ciliary localised Ca²⁺-permeable ion channel PKD2L1 exhibit defects in the IFT-dependent trafficking of the Shh transcription factor Gli2 to the tip of the primary cilium (Delling et al., 2013). In *Chlamydomonas*, phosphorylation of the FLA8 kinesin subunit by the Ca²⁺-dependent protein kinase CDPK1 blocks FLA8 entry into the flagellum and promotes dissociation of kinesin from the IFT particles at the ciliary tip, suggesting a role for Ca²⁺ in cargo unloading (Liang et al., 2014).

Ca²⁺ has also been implicated in the movement of flagella membrane proteins in *Chlamydomonas*. An adhesive glycoprotein in the flagella membrane (FMG-1B) allows *Chlamydomonas* cells to adhere to substrates (Bloodgood, 1981, 2009; Bloodgood and Workman, 1984; Xu et al., 2020). Transient interactions between FMG-1B and IFT particles direct the movement of FMG-1B along the flagella, as demonstrated by the co-localisation of individual IFT trains with polystyrene microspheres moving along the flagella surface (Shih et al., 2013). This process is utilised to drive gliding motility in *Chlamydomonas*, where the cell moves along a surface on its adherent flagella. The motile force is provided by the retrograde movement of FMG-1B along the flagellum, which results in the flagellum pulling the cell body forward (Bloodgood, 1995, 2009). Gliding motility is therefore caused by transient associations between FMG-1B and retrograde IFT particles, representing an excellent system in which to study dynamic interactions between cargo proteins and IFT particles.

¹Marine Biological Association, The Laboratory, Citadel Hill, Plymouth PL1 2PB, UK.

²School of Ocean and Earth Science, University of Southampton, Southampton SO14 3ZH, UK.

*Author for correspondence (glw@mba.ac.uk)

 G.W., 0000-0002-4657-1701

Handling Editor: David Stephens

Received 27 August 2020; Accepted 5 January 2021

Gliding motility is regulated by Ca^{2+} , requiring micromolar Ca^{2+} in the external medium (Bloodgood and Salomonsky, 1990). Bead movement is also inhibited by the absence of Ca^{2+} or by the presence of diltiazem, an inhibitor of voltage-gated Ca^{2+} channels (Bloodgood and Salomonsky, 1990). The implication that IFT motors are involved in gliding suggests that Ca^{2+} most likely acts to regulate the interaction between IFT and FMG-1B. Shih et al. (2013) found that chelating external Ca^{2+} reduced the pausing frequency of IFT trains, suggesting that Ca^{2+} was required for the interaction between FMG-1B and IFT particles. In contrast, Collingridge et al. (2013) found that the absence of external Ca^{2+} led to a substantial accumulation of IFT particles in adherent flagella, suggesting that Ca^{2+} acts to disrupt rather than promote the interaction between FMG-1B and the IFT particle. This was supported by simultaneous imaging of intraflagellar Ca^{2+} ($[\text{Ca}^{2+}]_{\text{fla}}$) and IFT using biolistically-loaded dextran-conjugated Ca^{2+} -responsive fluorescent dyes, which showed that $[\text{Ca}^{2+}]_{\text{fla}}$ elevations acted to initiate the movement of paused IFT particles.

The discrepancy between these two findings cannot easily be resolved, yet it clearly indicates that greater understanding of the interaction between $[\text{Ca}^{2+}]_{\text{fla}}$ and IFT is required. In particular, the processes leading to the pausing and accumulation of IFT trains remain unclear. Direct evidence for a regulatory function for $[\text{Ca}^{2+}]_{\text{fla}}$ in the interaction between FMG-1B and the IFT particle is also currently lacking. Detailed examination of the spatial and temporal organisation of Ca^{2+} elevations in relation to IFT events is therefore necessary, but requires a system in which flagella can be immobilised without inhibiting Ca^{2+} signalling. The potential requirement for Ca^{2+} in other aspects of IFT must also be examined.

Ca^{2+} -dependent signalling processes also contribute to many other flagella functions in *Chlamydomonas*, such as changes in flagella beat and waveform during motile responses, flagella adhesion during mating, flagella excision and flagella length control (Goodenough et al., 1993; Hegemann and Berthold, 2009; Quarmby, 1996; Wheeler, 2017). A detailed study of flagella Ca^{2+} dynamics will help us understand how specificity is achieved for a particular signalling role. In this study, we have analysed the interactions between $[\text{Ca}^{2+}]_{\text{fla}}$ and IFT in adherent *Chlamydomonas* flagella, using genetically encoded Ca^{2+} reporters targeted to the flagella. We demonstrate that intraflagellar Ca^{2+} elevations act to regulate the accumulation of paused retrograde IFT particles, by promoting their dissociation from the flagella membrane, but we do not find evidence for a role for $[\text{Ca}^{2+}]_{\text{fla}}$ elevations in other IFT processes. We also reveal complex spatiotemporal characteristics of Ca^{2+} in *Chlamydomonas* flagella, such as high-frequency repetitive Ca^{2+} spiking and the presence of localised or propagating $[\text{Ca}^{2+}]_{\text{fla}}$ elevations, which indicate that Ca^{2+} acts locally in its interaction with IFT. By regulating the interaction between IFT and FMG-1B, $[\text{Ca}^{2+}]_{\text{fla}}$ elevations play an important role in modulating flagella adhesion, in addition to regulating gliding motility.

RESULTS

Distinct forms of paused IFT particles in *Chlamydomonas* flagella

We have previously observed that accumulations of paused IFT trains are associated with gliding motility in adherent flagella (Collingridge et al., 2013). However, the origin and nature of the paused IFT trains was not examined in detail. Using total internal reflection fluorescence (TIRF) microscopy of a *Chlamydomonas* reporter strain expressing IFT54–mScarlet (strain IFT54-MS), we found that paused IFT trains could be designated into two clear categories (Fig. 1A–C). The first of these consisted of paused

anterograde IFT particles, which remain highly localised and usually only paused for a short period before continuing in an anterograde direction (Fig. 1B). Paused anterograde IFT trains have been observed to disrupt the movement of other anterograde IFT trains, but do not interfere with retrograde transport (Stepanek and Pigino, 2016). The second category of paused IFT trains was primarily observed in the distal region of the flagellum and had a longer mean pausing duration (Fig. 1C; Fig. S1A,B). The region of paused IFT trains slowly expanded in size (mean±s.e.m. maximal length of $1.81\pm 0.35\ \mu\text{m}$, $n=9$) and fluorescence intensity over time, indicating that additional IFT trains continue to pause in these regions. The paused IFT trains were periodically cleared by retrograde transport, suggesting that they represent paused retrograde IFT trains (Fig. 1C). This was supported by the presence of similar distal accumulations of IFT trains in a reporter strain for the dynein light intermediate chain (D1bLIC) of cytoplasmic dynein 1b (the retrograde IFT motor) (Reck et al., 2016) (Fig. 1D), whereas similar accumulations were absent in a reporter strain for the KAP subunit of kinesin (the anterograde IFT motor) (Collingridge et al., 2013; Mueller et al., 2005). As kinesin returns to the cell body via diffusion and is not present in retrograde IFT trains (Chien et al., 2017), the distal accumulations are likely to be formed by paused retrograde IFT trains.

The diffuse nature of the distal IFT accumulations and their formation in distal regions close to the flagella tip made it difficult to observe whether they are formed directly by paused retrograde IFT trains. However, it was possible to observe how additional IFT trains contributed to these accumulations, using a fluorescence recovery after photobleaching (FRAP) approach. Flagella exhibiting clear distal IFT accumulations were selected for photobleaching. After bleaching, individual anterograde IFT trains could be observed to proceed through the distal region to reach the flagella tip (examination of the three initial anterograde trains after each bleaching event showed that 42 out of 45 anterograde IFT trains clearly reached the flagella tip, $n=15$ flagella) (Fig. 1E; Fig. S1C,D). Following their arrival at the flagella tip, distinct retrograde transport of these IFT trains was not observed. However, accumulations of paused IFT trains began to form in the distal region close to the flagella tip immediately after their arrival. The increase in paused IFT trains is therefore due to additional IFT trains arriving at the distal end of the accumulation, rather than anterograde IFT trains adding to the accumulation at its proximal end. As the fluorescent IFT trains accumulate close to the flagella tip, we could not clearly determine whether they had undergone remodelling into retrograde IFT trains. However, as kinesin does not contribute to distal IFT accumulations, it seems likely that these IFT trains have transitioned into retrograde IFT trains, but cannot move away from the tip due to the large number of bleached retrograde IFT trains that have already paused in the distal region. The unimpeded progression of anterograde IFT trains through the distal region is consistent with observations that anterograde and retrograde IFT trains travel on distinct microtubules within each doublet (Stepanek and Pigino, 2016).

Development of a flagella-targeted Ca^{2+} sensor in *Chlamydomonas*

To further examine the role of $[\text{Ca}^{2+}]_{\text{fla}}$ elevations in regulating IFT pausing and other events, we targeted a genetically encoded Ca^{2+} -sensitive reporter protein (G-GECO1.1) to *Chlamydomonas* flagella. We fused G-GECO to the C-terminus of CAH6, an abundant carbonic anhydrase that is associated with the flagella membrane (Fig. 2A) (Engel et al., 2012; Liu and Lechtreck, 2018;

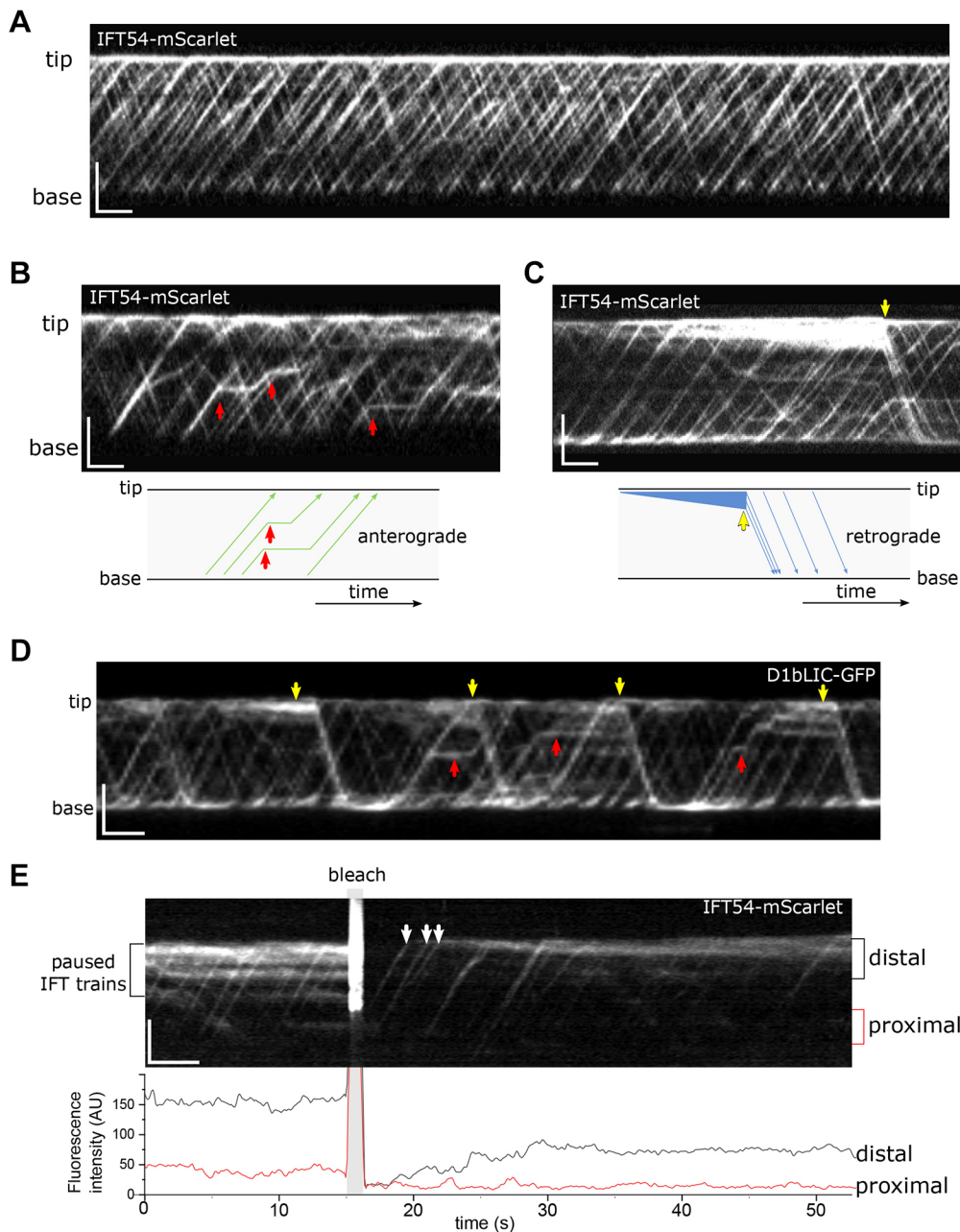


Fig. 1. Distinct forms of paused IFT trains in *Chlamydomonas* flagella. (A) Kymograph of IFT54–mScarlet indicating movement of IFT trains. Anterograde IFT trains move towards the flagella tip and retrograde trains return to the base of the flagellum. (B) Kymograph indicating pausing of anterograde IFT trains. Anterograde IFT trains pause (red arrows) and then continue in an anterograde direction. (C) Kymograph indicating pausing of retrograde IFT trains. Paused IFT trains accumulate in the distal region of the flagellum. The initiation of retrograde movement occurs at a single time point (yellow arrow). (D) Kymograph of D1bLIC–GFP showing a series of distal accumulations that are cleared by retrograde movement (yellow arrows). (E) Photobleaching of paused IFT54–mScarlet to allow visualisation of subsequent IFT trains entering the flagellum. After bleaching, fluorescent anterograde IFT trains reach the flagella tip (arrow), but do not exhibit subsequent retrograde transport through the region of paused IFT trains. The graph shows the fluorescence intensity in the proximal and distal regions. Similar results were obtained on 33 flagella. Scale bars: 5 μ m (vertical) and 10 s (horizontal).

Mackinder et al., 2017). CAH6 shows an even distribution along the length of the flagellum, although it is more abundant in the *trans*- rather than the *cis*-flagellum (Yu et al., 2020). Using this approach, we were able to successfully target G-GECO to the flagella of *Chlamydomonas* strain CC-5325 (to produce strain GG-WT). TIRF microscopy of adherent flagella revealed that $[Ca^{2+}]_{na}$ elevations were associated with gliding movement. $[Ca^{2+}]_{na}$ elevations were observed in 94.8% of trailing flagella at the onset of the gliding motility ($n=116$), but were largely absent from leading flagella (Fig. 2B–D; Movie 1), strongly supporting previous observations of gliding-related $[Ca^{2+}]_{na}$ elevations using biolistically loaded Ca^{2+} -responsive fluorescent dyes (Oregon Green–BAPTA–dextran; OGB) (Collingridge et al., 2013). Cells expressing CAH6–Venus did not exhibit any changes in fluorescence during gliding motility, indicating that the rapid changes in G-GECO fluorescence were not due to motion artefacts (Fig. S2).

We next examined the influence of different surface properties on flagella Ca^{2+} signalling. We have previously used 0.01% poly-L-lysine to promote flagella adhesion without inhibiting gliding motility (Collingridge et al., 2013). Much higher concentrations of poly-L-lysine (>1%) can completely immobilise flagella, but can also lead to deflagellation, indicating that care is required when increasing adhesion (Dentler et al., 2009; Engel et al., 2009). On non-treated glass coverslips, many cells moved excessively or lifted their flagella from the surface within a relatively short period, although a proportion remained attached throughout the imaging period (2 min). We found that $[Ca^{2+}]_{na}$ elevations in these flagella were associated primarily with movement during gliding motility (Fig. 3A). Treatment of the glass coverslip with 0.1% poly-L-lysine greatly reduced gliding motility and flagella lifting, indicating that many of the flagella were unable to overcome the increased adhesion to the surface. The immobilised adherent flagella often

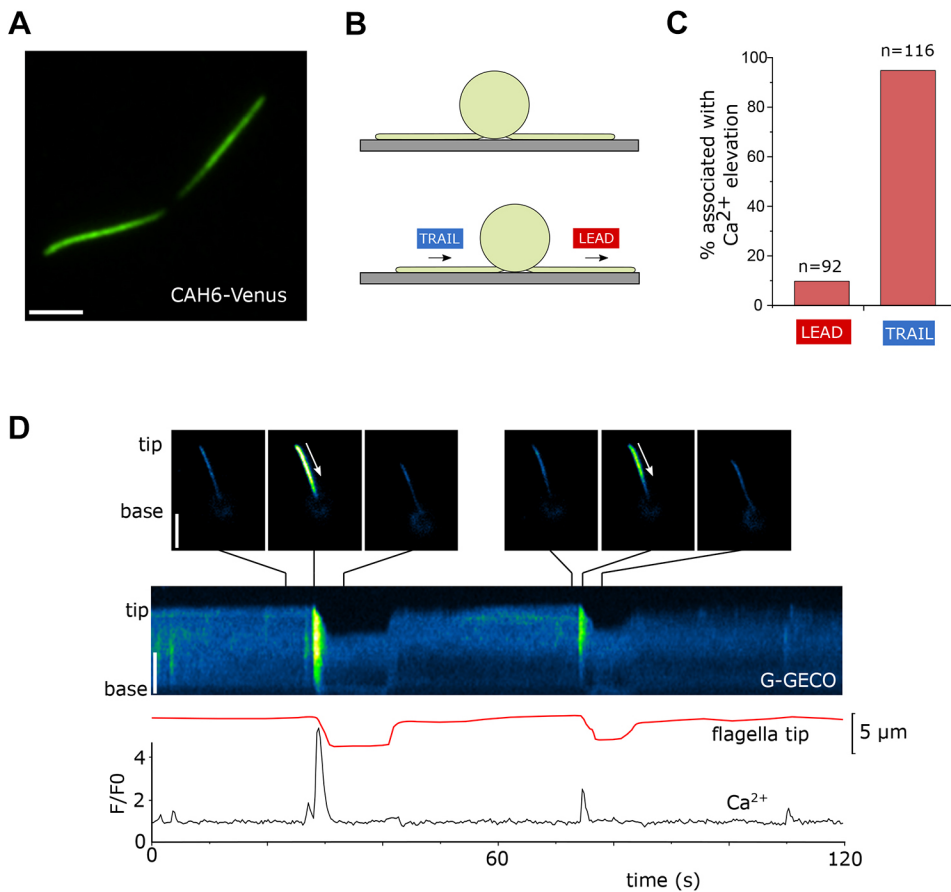


Fig. 2. Development of a flagella-targeted Ca^{2+} sensor in *Chlamydomonas*.

(A) Adherent flagella in a cell expressing CAH6–Venus, viewed by TIRF microscopy. (B) *Chlamydomonas* cells with adherent flagella. (C) Quantification of $[\text{Ca}^{2+}]_{\text{fla}}$ elevations associated with flagella movements. The percentage of gliding movements (leading and trailing) that coincide with a $[\text{Ca}^{2+}]_{\text{fla}}$ elevation. (D) Kymograph illustrating flagella Ca^{2+} ($[\text{Ca}^{2+}]_{\text{fla}}$) elevations during gliding motility in a wild-type strain expressing CAH6–G-GECO (GG-WT strain). Substantial $[\text{Ca}^{2+}]_{\text{fla}}$ elevations are associated with dragging movements but not with forward movements. The red line indicates the position of the flagella tip in order to highlight gliding movements. White arrow indicates direction of gliding movement. Scale bars: 5 μm .

exhibited repetitive $[\text{Ca}^{2+}]_{\text{fla}}$ elevations, with frequencies up to 0.57 Hz (Fig. 3B); 63.6% of flagella on poly-L-lysine-treated coverslips exhibited high-frequency Ca^{2+} elevations (greater than 0.17 Hz), compared to 8.3% of flagella on untreated coverslips (Fig. 3C). The repetitive $[\text{Ca}^{2+}]_{\text{fla}}$ elevations were not associated with motility, but occurred in immobilised flagella that were strongly adhered to the poly-L-lysine-treated surface. Removing external Ca^{2+} strongly inhibited the repetitive $[\text{Ca}^{2+}]_{\text{fla}}$ elevations, indicating that they require Ca^{2+} influx across the flagella membrane (Fig. 3D). Removing external Ca^{2+} also inhibited gliding motility, as observed previously (Bloodgood and Salomonsky, 1990; Collingridge et al., 2013). The adhesive properties of the surface therefore have an important influence on Ca^{2+} signalling within *Chlamydomonas* flagella.

$[\text{Ca}^{2+}]_{\text{fla}}$ elevations coincide with the movement of paused retrograde IFT accumulations

Previously, we have demonstrated that the $[\text{Ca}^{2+}]_{\text{fla}}$ elevations observed in trailing flagella during the onset of gliding motility are associated with the retrograde movement of paused IFT trains (Collingridge et al., 2013). However, flagella exhibiting extensive gliding movements are difficult to image over longer periods, preventing detailed assessment of the interactions between $[\text{Ca}^{2+}]_{\text{fla}}$ elevations and IFT. To address this, we expressed G-GECO in the IFT54-MS reporter strain and imaged flagella immobilised on 0.1% poly-L-lysine-treated coverslips. Flagella exhibiting a very high frequency of $[\text{Ca}^{2+}]_{\text{fla}}$ elevations (>0.25 Hz) were excluded from this initial analysis to prevent false correlations with high-frequency IFT events (e.g. entry of IFT trains occurs at 1–1.3 Hz; Wingfield

et al., 2017). Regular IFT events, such as the entry of anterograde IFT trains into the flagellum, the arrival of anterograde IFT trains at the flagella tip and the departure of retrograde IFT trains from the flagella tip, did not show a close relationship with $[\text{Ca}^{2+}]_{\text{fla}}$, as they occurred both in the presence and absence of $[\text{Ca}^{2+}]_{\text{fla}}$ elevations (Fig. 4A,B). We also found no evidence for a correlation between elevated $[\text{Ca}^{2+}]_{\text{fla}}$ and the pausing or restarting of anterograde IFT trains. We were unable to clearly resolve the timing at which individual retrograde IFT trains paused, although it was clear that the initiation of the distal IFT accumulations occurs in periods lacking $[\text{Ca}^{2+}]_{\text{fla}}$ elevations (Fig. 4A). However, the restart of paused retrograde IFT trains showed a close association with elevated $[\text{Ca}^{2+}]_{\text{fla}}$ (Fig. 4A,B); 90.2% of these events coincided with the onset of a $[\text{Ca}^{2+}]_{\text{fla}}$ elevation (defined as occurring within 0.5 s, $n=41$ events), whereas other IFT events only rarely coincided with the onset of $[\text{Ca}^{2+}]_{\text{fla}}$ elevations (Fig. 4C,D).

We also examined the impact of $[\text{Ca}^{2+}]_{\text{fla}}$ elevations on the velocity of IFT trains. The mean velocity of anterograde IFT trains was not influenced by elevated $[\text{Ca}^{2+}]_{\text{fla}}$, but there was a slight increase (+12.4%) in the velocity of retrograde IFT trains in the presence of elevated $[\text{Ca}^{2+}]_{\text{fla}}$ (Fig. 4E). This may indicate a reduction in transient pausing of retrograde IFT trains during $[\text{Ca}^{2+}]_{\text{fla}}$ elevations.

We conclude that $[\text{Ca}^{2+}]_{\text{fla}}$ elevations in adherent flagella play an important role in initiating the movement of paused retrograde IFT trains. We find no evidence for a direct requirement for $[\text{Ca}^{2+}]_{\text{fla}}$ elevations in other IFT processes, such as the entry and turnaround of IFT trains or the pausing of anterograde IFT trains. This suggests that rapid $[\text{Ca}^{2+}]_{\text{fla}}$ elevations do not directly regulate these other

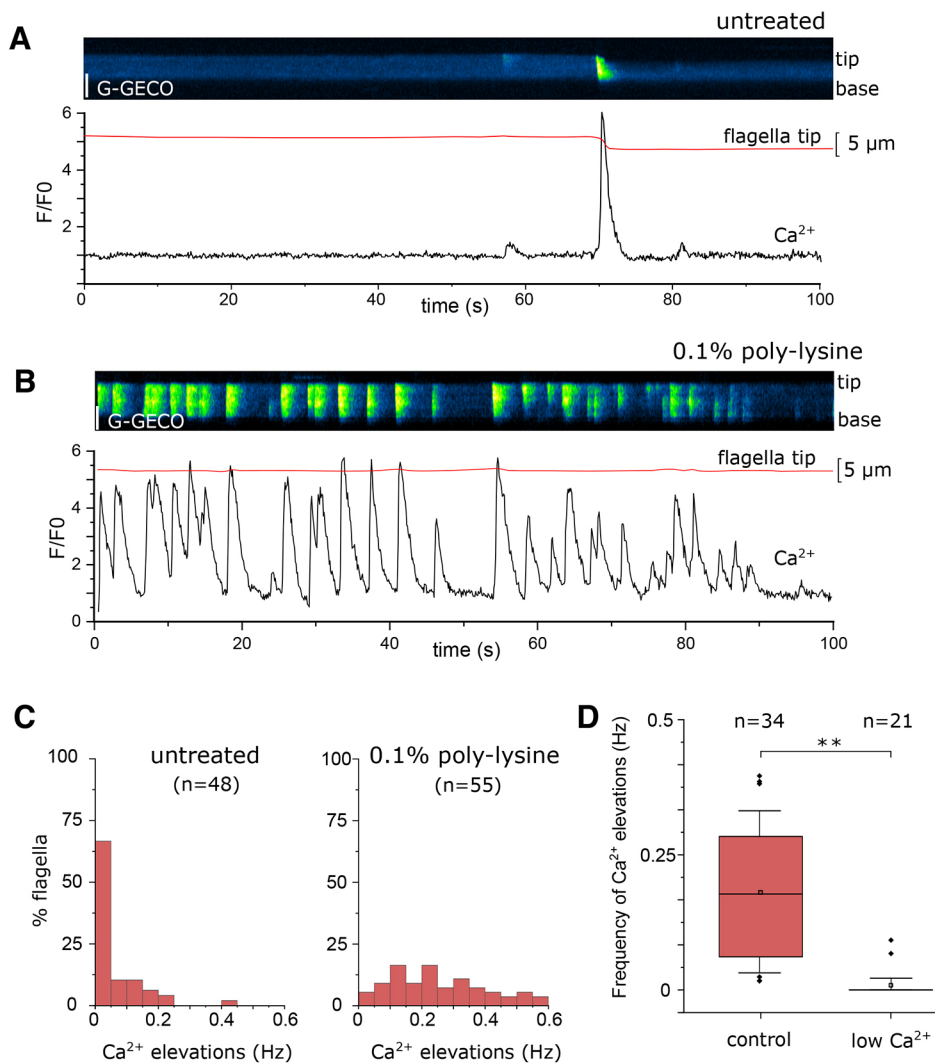


Fig. 3. Increased adhesion results in high-frequency Ca²⁺ spiking within flagella. (A) [Ca²⁺]_{fla} elevations in a flagellum adhering to a non-treated glass coverslip (GG-IFT54MS strain). (B) [Ca²⁺]_{fla} elevations in a flagellum adhering to a coverslip treated with 0.1% poly-L-lysine. Scale bars: 5 μm. (C) Frequency histograms showing the percentage of flagella exhibiting different frequencies of [Ca²⁺]_{fla} elevations. *n*=48 untreated, *n*=55 0.1% poly-L-lysine; bin size, 0.05 Hz. (D) Repetitive [Ca²⁺]_{fla} elevations require external Ca²⁺. The frequency of [Ca²⁺]_{fla} elevations in GG-IFT54MS cells after 20 min in different concentrations of external Ca²⁺. *n*=34 control, *n*=21 low Ca²⁺. Box plots show the 25–75th percentiles with median, mean is the open square and whiskers represent 10–90th percentiles. ***P*<0.01 (paired *t*-test).

IFT processes, although our analyses cannot rule out a potential regulatory role for Ca²⁺ via alternative mechanisms. For example, Ca²⁺-dependent protein kinases have been implicated in the dissociation of kinesin from IFT particles at the flagella tip during IFT turnover (Liang et al., 2014). As gradients in resting cytosolic Ca²⁺ can be observed in some cells, notably in polarised plant cells such as root hairs or pollen tubes (Foreman et al., 2003; Steinhorst and Kudla, 2013), we investigated whether resting [Ca²⁺]_{fla} differed at the flagella tip. The median intensity of CAH6–G-GECO or CAH6–Venus (as a non-Ca²⁺-responsive control) did not differ along the length of the flagellum (Fig. S3A,B). We also examined cells that had been biolistically loaded with the Ca²⁺-responsive dye OGB and the non-Ca²⁺-responsive dye Texas Red dextran (TR), enabling ratiometric imaging of [Ca²⁺]_{fla}. The ratio of OGB/TR was similar along the length of the flagellum, indicating that resting [Ca²⁺]_{fla} is not consistently elevated at the flagella tip relative to the rest of the flagellum (Fig. S3C).

Repetitive [Ca²⁺]_{fla} elevations prevent distal IFT accumulations in adherent flagella

We previously observed a correlation between the frequency of [Ca²⁺]_{fla} elevations and the frequency of retrograde IFT, with retrograde IFT trains less frequent in flagella exhibiting few [Ca²⁺]_{fla}

elevations (Collingridge et al., 2013). This suggests that the observed differences in Ca²⁺ signalling between flagella on untreated and poly-L-lysine-treated surfaces (Fig. 3) may also influence the dynamics of IFT. Simultaneous observation of [Ca²⁺]_{fla} and IFT showed that the movement of IFT trains was highly regular in flagella on a 0.1% poly-L-lysine-treated surface, with a high frequency of anterograde and retrograde IFT trains, corresponding to the high frequency of [Ca²⁺]_{fla} elevations (Fig. 5A–C). In contrast, flagella on an untreated surface exhibited distal accumulations of paused IFT trains, and IFT appeared more disordered, with a lower frequency of anterograde and retrograde IFT trains. The accumulation of paused retrograde IFT trains likely contributes to the reduced frequency of retrograde IFT.

Examination of flagella on a 0.1% poly-L-lysine-treated surface exhibiting intermittent periods of repetitive [Ca²⁺]_{fla} elevations, allowed us to observe how transitions from quiescence to high-frequency Ca²⁺ spiking influenced pausing of retrograde IFT. Distal accumulations of retrograde IFT trains were observed in all flagella during the quiescent period (*n*=10) (Fig. 5D,E; Movies 2, 3). These were rapidly dispersed at the onset of high-frequency [Ca²⁺]_{fla} elevations and further retrograde IFT trains did not pause and accumulated in flagella where high-frequency [Ca²⁺]_{fla} elevations persisted. The pausing and restarting of anterograde IFT trains was not affected by the transition between quiescence and rapid Ca²⁺

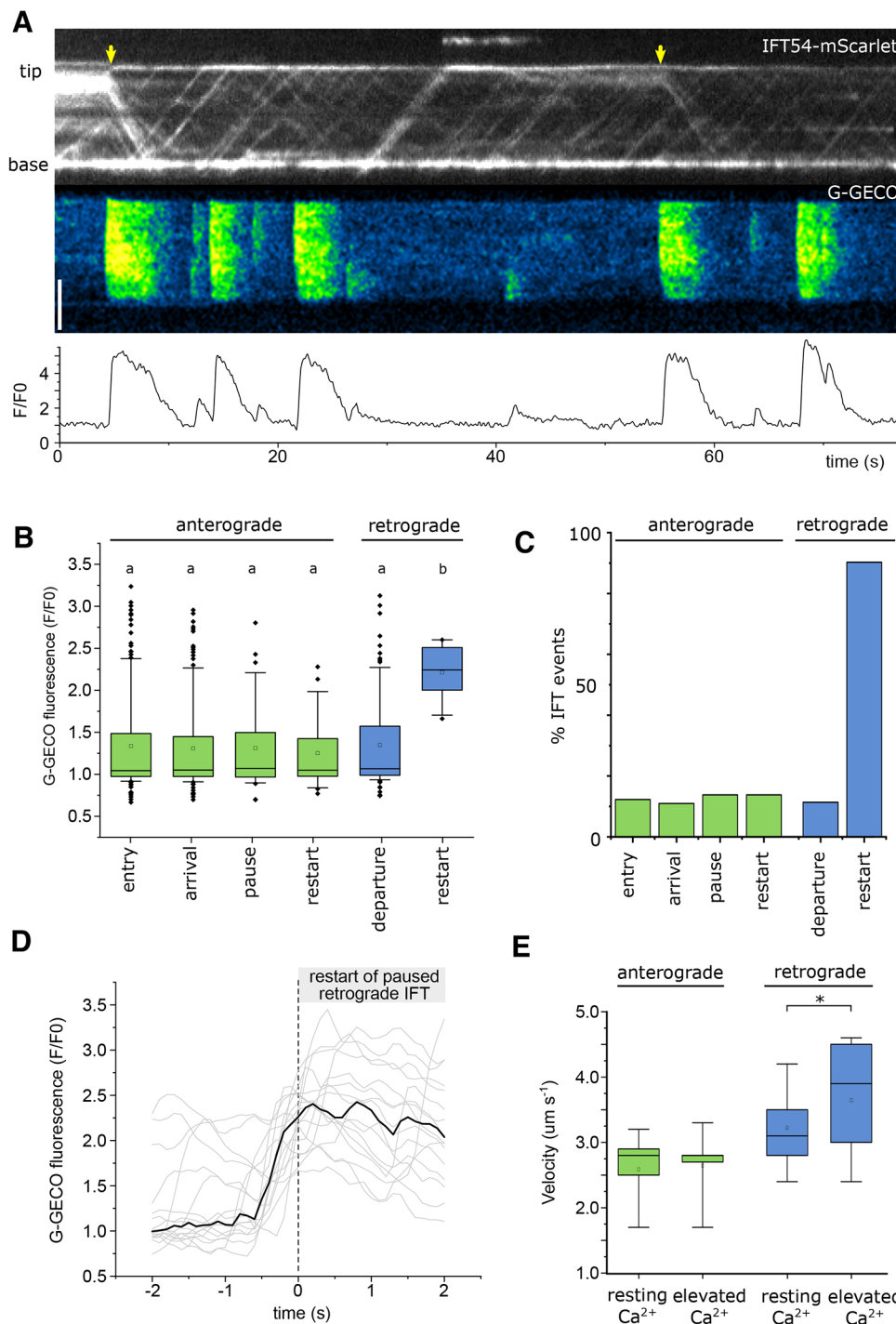


Fig. 4. $[\text{Ca}^{2+}]_{\text{fla}}$ elevations coincide with retrograde movement of distal IFT accumulations. (A) The kymographs indicate the movement of IFT54 (upper) and changes in $[\text{Ca}^{2+}]_{\text{fla}}$ (lower) in a flagellum adhering to a 0.1% poly-L-lysine-treated coverslip. Yellow arrows indicate movement of paused retrograde IFT trains. Scale bar: 5 μm . (B) Box plot showing $[\text{Ca}^{2+}]_{\text{fla}}$ (displayed as relative G-GECO fluorescence) at the time of each IFT event. Anterograde IFT events are entry into flagellum, arrival at flagella tip, pausing and restarting of anterograde IFT. Retrograde IFT events are departure from flagella tip, restarting of paused retrograde IFT. $n=154$, 133, 32, 22, 92 and 17, respectively. Means not sharing a letter are significantly different from one another ($P<0.05$, one-way ANOVA, Tukey post hoc test). (C) Frequency histogram illustrating the percentage of each IFT event that was observed to coincide with the initiation of a $[\text{Ca}^{2+}]_{\text{fla}}$ elevation. $n=1023$, 82, 29, 29, 773 and 41 IFT events for each category, respectively. (D) Timing of $[\text{Ca}^{2+}]_{\text{fla}}$ elevations associated with restart of paused retrograde IFT. 17 events are shown from six individual cells. Bold line, median trace; individual traces are shown in grey. (E) Box plot showing the velocity of IFT trains during $[\text{Ca}^{2+}]_{\text{fla}}$ elevations (i.e. while $[\text{Ca}^{2+}]_{\text{fla}}$ was elevated above resting), relative to the velocity in the absence of a $[\text{Ca}^{2+}]_{\text{fla}}$ elevation. $n=9$ flagella, with 200–410 IFT trains analysed for each category. $*P<0.05$ (paired t -test). Box plots show the 25–75th percentiles with median, mean is the open square and whiskers represent 10th and 90th percentiles.

spiking (Fig. 5D,E). The results indicate that paused retrograde IFT trains accumulate in the distal region of the flagellum in the absence of $[\text{Ca}^{2+}]_{\text{fla}}$ elevations and that high-frequency $[\text{Ca}^{2+}]_{\text{fla}}$ elevations prevent this accumulation.

To test this hypothesis, we inhibited flagella Ca^{2+} signalling through the removal of external Ca^{2+} . Paused retrograde IFT trains did not accumulate in the distal region of flagella exhibiting repetitive $[\text{Ca}^{2+}]_{\text{fla}}$ elevations (Fig. 6A,B; Fig. S4). Perfusion with a Ca^{2+} -free buffer resulted in the cessation of the $[\text{Ca}^{2+}]_{\text{fla}}$ elevations within 60 s of the onset of the perfusion. The inhibition of Ca^{2+} signalling led to a rapid accumulation of IFT trains in the distal

region of the flagella, with a 2.58 ± 0.25 -fold (mean \pm s.e.m.) increase in IFT20-mCherry fluorescence in this region observed 60 s after the inhibition of signalling ($n=8$ flagella). These observations confirm that high-frequency $[\text{Ca}^{2+}]_{\text{fla}}$ elevations act to prevent paused retrograde IFT trains accumulating in the distal regions of adherent flagella.

Whereas the frequency of retrograde IFT trains rapidly decreased following the inhibition of $[\text{Ca}^{2+}]_{\text{fla}}$ elevations, the frequency of anterograde IFT was not reduced initially (Fig. 6B). However, inhibition of flagella Ca^{2+} signalling over longer periods does lead to a reduced frequency of anterograde IFT (Collingridge et al.,

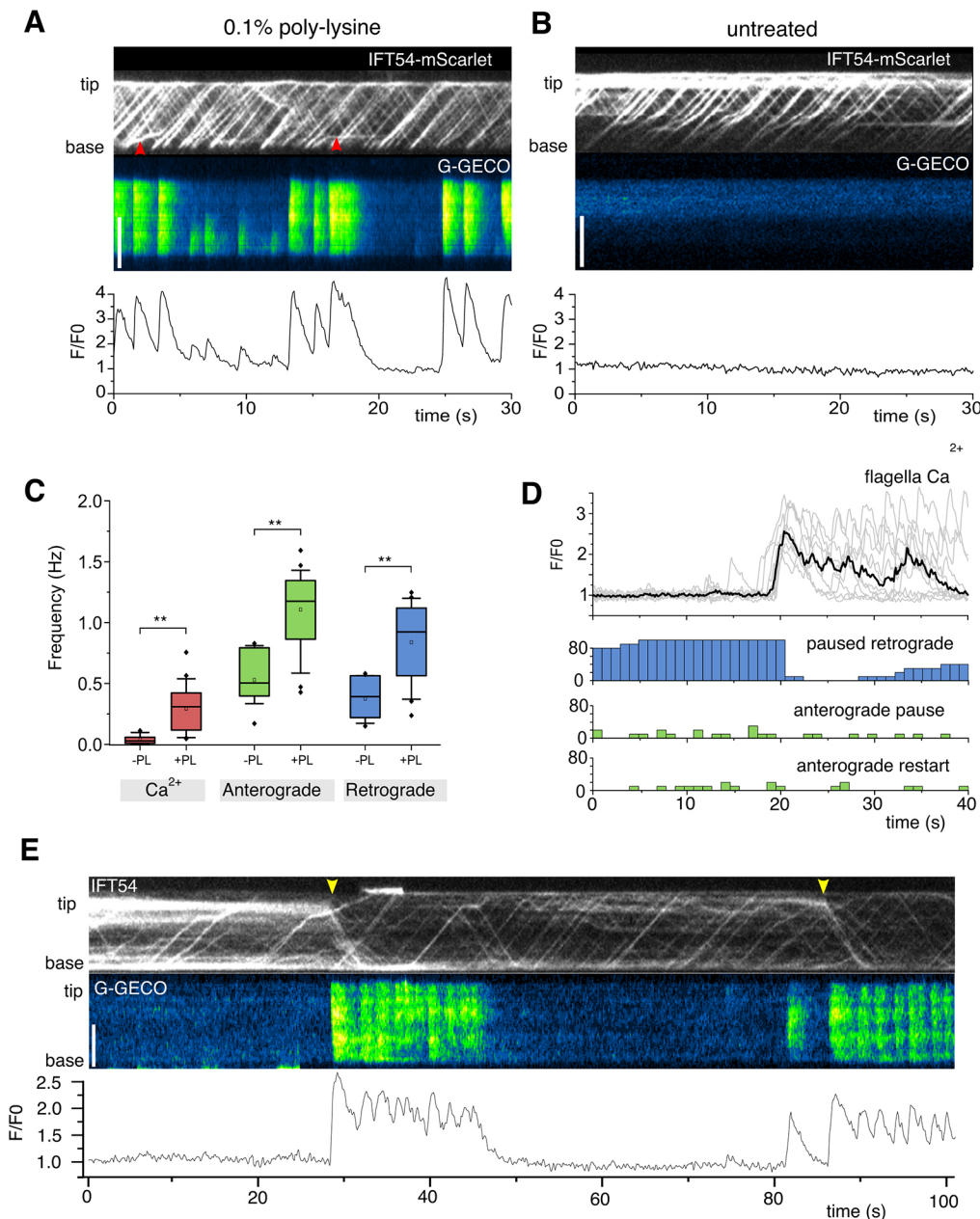


Fig. 5. Flagella exhibiting high-frequency $[Ca^{2+}]_{fla}$ elevations do not exhibit distal IFT accumulations.

(A) Simultaneous TIRF imaging of $[Ca^{2+}]_{fla}$ and IFT54-mScarlet on a 0.1% poly-L-lysine-treated surface. Flagella exhibit highly repetitive $[Ca^{2+}]_{fla}$ elevations. Pausing of anterograde IFT trains can still be observed (red arrows). Scale bar: 5 μ m. (B) As in A but on an untreated surface. (C) Box plots, presented as described in the Materials and Methods section, showing the frequency of $[Ca^{2+}]_{fla}$ elevations, anterograde IFT and retrograde IFT on untreated (-PL) and 0.1% poly-L-lysine-treated (+PL) surfaces ($n=11$ and 20 flagella, respectively). $**P<0.01$ between means (*t*-test).

(D) Pausing of IFT in flagella exhibiting intermittent high-frequency $[Ca^{2+}]_{fla}$ elevations. Traces have been aligned to show onset of $[Ca^{2+}]_{fla}$ elevations at 20 s. The histograms below show the percentage of flagella exhibiting accumulations of paused retrograde IFT, or the pausing or restarting of anterograde IFT trains. $n=10$ flagella. (E) A flagellum on a 0.1% poly-L-lysine-treated surface exhibiting intermittent $[Ca^{2+}]_{fla}$ elevations. In the absence of $[Ca^{2+}]_{fla}$ elevations, retrograde IFT trains accumulate in distal regions, but are cleared with the onset of $[Ca^{2+}]_{fla}$ elevations (yellow arrows). Scale bar: 5 μ m.

2013). As removing external Ca^{2+} causes a substantial overaccumulation of retrograde IFT trains in adherent flagella (Collingridge et al., 2013) (Fig. S5A,B), these retrograde IFT trains may accumulate to the extent that they impede the progression of anterograde IFT trains. This conclusion is seemingly at odds with the finding that anterograde and retrograde IFT trains travel on distinct microtubules and do not collide (Stepanek and Pigino, 2016). We therefore examined the nature of these large distal IFT accumulations using transmission electron microscopy (TEM) of flat-embedded adherent flagella. After the removal of external Ca^{2+} for 5 min, TEM of adherent flagella revealed large accumulations of IFT particles in the distal region, close to the flagella tip (Fig. S5C). This phenotype is similar to, but distinct from, the phenotype of mutants defective in retrograde IFT, which exhibit large accumulations of IFT trains at the flagella tip (Engel et al., 2012; Pazour et al., 1999). We propose that prolonged inhibition of

flagella Ca^{2+} signalling results in a massive accumulation of retrograde IFT trains behind the retrograde IFT trains that have already paused. In the absence of a mechanism to clear the paused retrograde IFT trains, they accumulate to an extent where they significantly impede the progress of anterograde IFT trains, even if these IFT trains move along a distinct microtubule track.

$[Ca^{2+}]_{fla}$ elevations disrupt microsphere movement along the flagellum

The pausing and accumulation of retrograde IFT trains likely reflects a direct interaction between the IFT particle and adhesive glycoproteins (predominately FMG-1B) in the flagella membrane. This interaction therefore represents a mechanism through which membrane proteins in contact with a surface can be tethered to the axoneme, allowing the generation of propulsive force via the retrograde motor, cytoplasmic dynein 1b. Our results strongly suggest that Ca^{2+} acts by regulating this

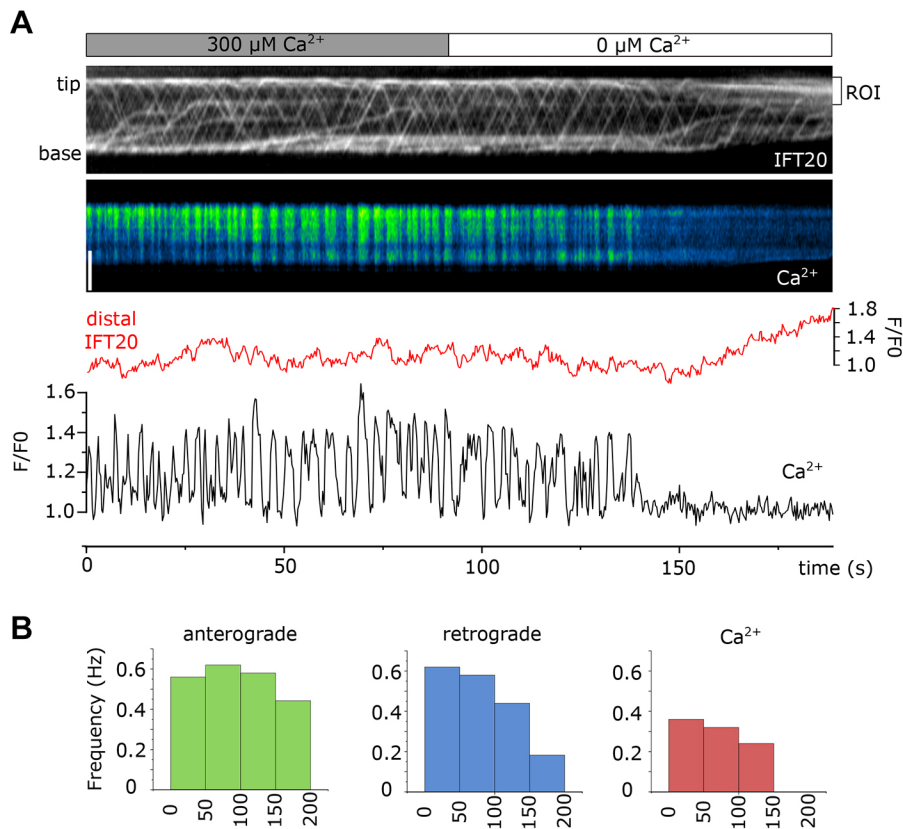


Fig. 6. Inhibition of $[\text{Ca}^{2+}]_{\text{fla}}$ elevations leads to the accumulation of IFT trains in distal region.

(A) The kymograph displays simultaneous imaging of IFT20-mCherry and OGB in a flagellum exhibiting repetitive $[\text{Ca}^{2+}]_{\text{fla}}$ elevations. The cell was initially perfused with a buffer containing 300 μM external Ca^{2+} , which was switched to a buffer containing 0 μM Ca^{2+} after 100 s. The absence of external Ca^{2+} inhibits $[\text{Ca}^{2+}]_{\text{fla}}$ elevations and leads to accumulation of IFT trains in the distal region of the flagellum (demonstrated by an increase of IFT20-mCherry fluorescence in the distal region, red trace). Note that pausing of anterograde IFT trains can occur during repetitive $[\text{Ca}^{2+}]_{\text{fla}}$ elevations. Scale bar: 5 μm . (B) Bar charts indicating the frequency of $[\text{Ca}^{2+}]_{\text{fla}}$ elevations, anterograde IFT and retrograde IFT throughout the time course shown in A.

interaction, thereby modulating the propulsive force generated by adherent flagella. The interaction between FMG-1B and IFT trains can be readily visualised by following the movement of fluorescent microspheres along the flagellum (Shih et al., 2013). Through simultaneous imaging of fluorescent microspheres and IFT27-GFP, we observed that microspheres stopped moving in a particular direction when the microsphere switched to an IFT train moving in the opposite direction or reached the end of the flagellum (Fig. 7A). However, on some occasions the microspheres could be observed to dissociate from the IFT train (anterograde or retrograde) and exhibit diffusional movement in the flagella membrane. We hypothesised that these events represent a disruption of the interaction between the IFT particle and FMG-1B, which could be mediated by $[\text{Ca}^{2+}]_{\text{fla}}$ elevations.

We therefore observed microsphere movements along a flagellum while simultaneously monitoring $[\text{Ca}^{2+}]_{\text{fla}}$. A total of 12 out of 25 flagella exhibiting IFT-driven microsphere movement also exhibited a $[\text{Ca}^{2+}]_{\text{fla}}$ elevation during this period. In each of these flagella, the $[\text{Ca}^{2+}]_{\text{fla}}$ elevation coincided directly with the cessation of microsphere movement, with the microsphere either subsequently exhibiting diffusional movement or becoming detached from the flagellum entirely (Fig. 7B–D; Movies 4, 5). We attribute the latter events to a strong attraction between the microsphere and the poly-L-lysine-treated surface. $[\text{Ca}^{2+}]_{\text{fla}}$ elevations disrupted microsphere movement at any position along the entire length of the flagellum, and the effect of Ca^{2+} was not restricted to microspheres in the distal region (Fig. 7B). Moreover, we did not observe microspheres moving on flagella that exhibited high-frequency $[\text{Ca}^{2+}]_{\text{fla}}$ elevations. We conclude that $[\text{Ca}^{2+}]_{\text{fla}}$ elevations act directly to disrupt the interaction between IFT trains and FMG-1B.

$[\text{Ca}^{2+}]_{\text{fla}}$ elevations have distinct spatial properties

Our findings indicate that the $[\text{Ca}^{2+}]_{\text{fla}}$ elevations observed in *Chlamydomonas* show complex temporal patterns that directly influence the movement of IFT trains. However, it is clear that $[\text{Ca}^{2+}]_{\text{fla}}$ elevations also demonstrate distinct spatial properties. In cells exhibiting lower frequency Ca^{2+} elevations (<0.25 Hz), 35.7% of the $[\text{Ca}^{2+}]_{\text{fla}}$ elevations were restricted to either the proximal or the distal region of the flagellum (Fig. 8A,B). Moreover, 28.1% of the $[\text{Ca}^{2+}]_{\text{fla}}$ elevations that spanned the length of the flagellum exhibited a substantial difference in the timing of their onset (>0.2 s) between the distal and proximal regions (Fig. 8C). Closer examination of these signalling events indicated that they resembled a Ca^{2+} wave that propagated along the length of the flagellum in either direction, with 43.8% propagating in a retrograde direction and 56.2% propagating in an anterograde direction. The mean rate of propagation was $28.7 \pm 4.3 \mu\text{m s}^{-1}$ (mean \pm s.e.m., $n=10$) (Fig. 8D).

The identification of spatially localised $[\text{Ca}^{2+}]_{\text{fla}}$ elevations allowed us to determine whether Ca^{2+} acted in a local or global manner to initiate the movement of paused retrograde IFT trains. We used the propagating $[\text{Ca}^{2+}]_{\text{fla}}$ elevations to examine whether the onset of movement of paused IFT trains in the distal region corresponded with the elevation of $[\text{Ca}^{2+}]_{\text{fla}}$ in either the distal or proximal region. We found that the movement of paused retrograde IFT trains corresponded closely to the time at which $[\text{Ca}^{2+}]_{\text{fla}}$ became elevated in the distal region, irrespective of whether the $[\text{Ca}^{2+}]_{\text{fla}}$ wave initiated in the distal or proximal region (Fig. 8E,F). This indicates that $[\text{Ca}^{2+}]_{\text{fla}}$ elevations act locally, requiring colocalisation with the paused retrograde IFT trains in order to initiate their movement.

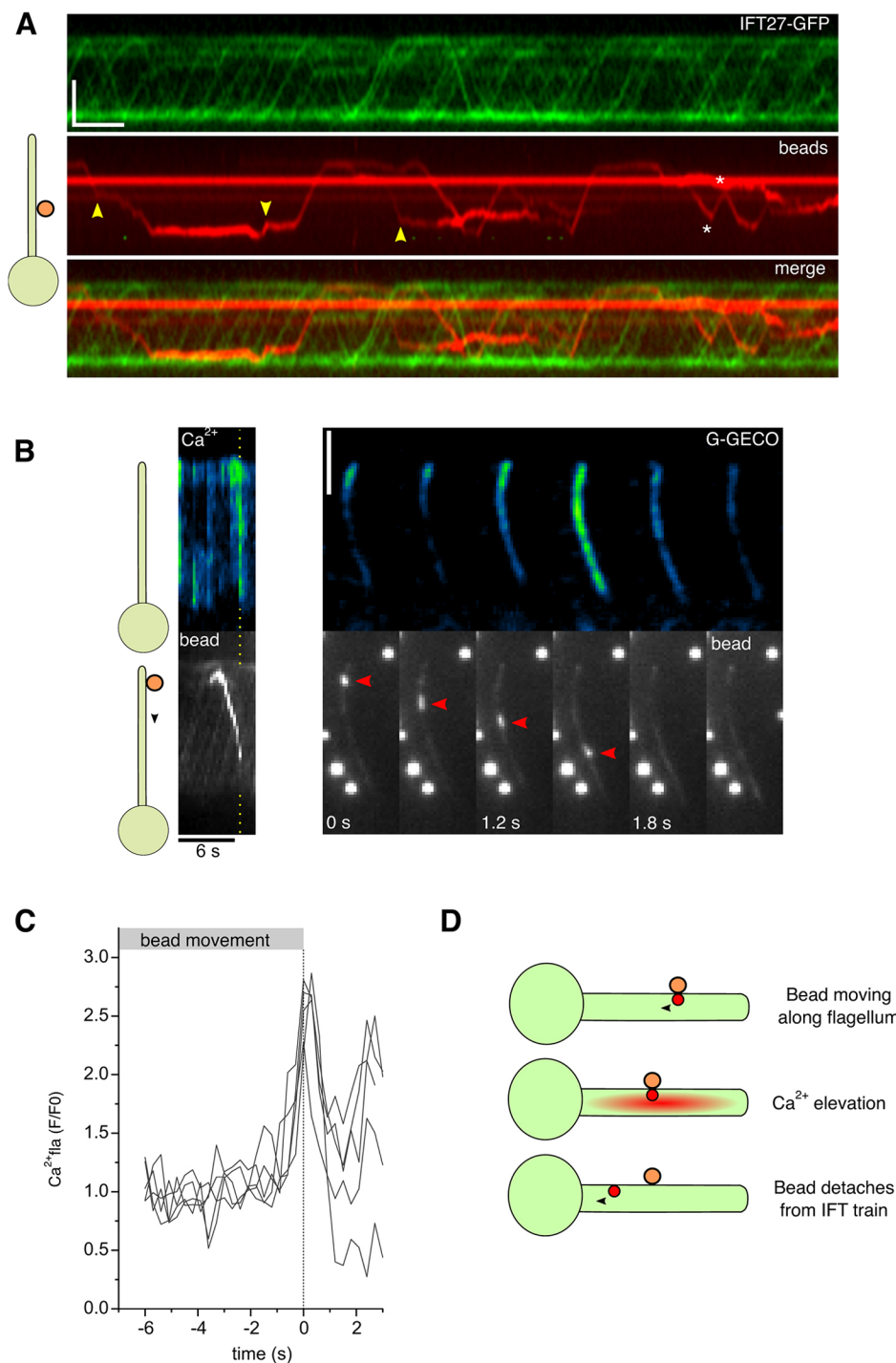


Fig. 7. $[\text{Ca}^{2+}]_{\text{fla}}$ elevations inhibit movement of microspheres along the flagellum.

(A) Kymograph displaying simultaneous TIRF imaging of IFT27-GFP and fluorescent microspheres. Microspheres moving in both anterograde and retrograde directions colocalise with IFT trains. Yellow arrows indicate events where microspheres dissociate from the IFT train and exhibit diffusive movement. Asterisks indicate events where microspheres rapidly change direction by associating to IFT trains moving in the opposite direction. Scale bars: 5 μm (vertical) and 10 s (horizontal). (B) Kymograph displaying simultaneous TIRF imaging of $[\text{Ca}^{2+}]_{\text{fla}}$ and fluorescent microspheres. The image sequence demonstrates that the $[\text{Ca}^{2+}]_{\text{fla}}$ elevation coincides directly with the end of movement of the microsphere (arrowed), which in this case is lost from the flagellum. Scale bar: 5 μm (vertical). Diagrams on left of A, B show position of flagellum relative to the cell body. (C) $[\text{Ca}^{2+}]_{\text{fla}}$ elevations in flagella displaying IFT-driven microsphere movement. $[\text{Ca}^{2+}]_{\text{fla}}$ traces are shown relative to the cessation of IFT-driven microsphere movement ($n=5$ flagella). (D) Schematic displaying the proposed signalling events involved in the detachment of microspheres from IFT trains.

Detachment from a surface requires external Ca^{2+}

Recent observations indicate that the adhesive properties of *Chlamydomonas* flagella are highly dynamic, with blue light promoting rapid changes in flagella adhesion to a surface (Kreis et al., 2019, 2018). As light-dependent modulation of adhesion appears to involve a redistribution of FMG-1B along the flagella surface (Kreis et al., 2018), interactions between FMG-1B and IFT may also contribute to adhesion. Lifting of flagella from a surface is often initiated by axonemal bending in the non-adherent region of the flagellum, resulting in the flagellum being dragged towards the cell body so that only the tip remains adherent. We found that flagella lifting was strongly associated with $[\text{Ca}^{2+}]_{\text{fla}}$ elevations,

with both the GG-WT and GG-IFT54-MS strains routinely exhibiting a $[\text{Ca}^{2+}]_{\text{fla}}$ elevation at the onset of each lifting event (Fig. S6A,B). Detailed examination of the timing of lifting events revealed that, in all cases, the $[\text{Ca}^{2+}]_{\text{fla}}$ elevation immediately preceded the initial movement of the flagellum towards the cell body (Fig. S6C). We propose that the $[\text{Ca}^{2+}]_{\text{fla}}$ elevations act to release FMG-1B from paused retrograde IFT trains, which removes resistance to the pulling force generated by axonemal bending and allows the flagellum to be drawn towards the cell body and lifted from the surface.

We therefore examined whether Ca^{2+} -dependent removal of paused retrograde IFT trains was required for light-modulated

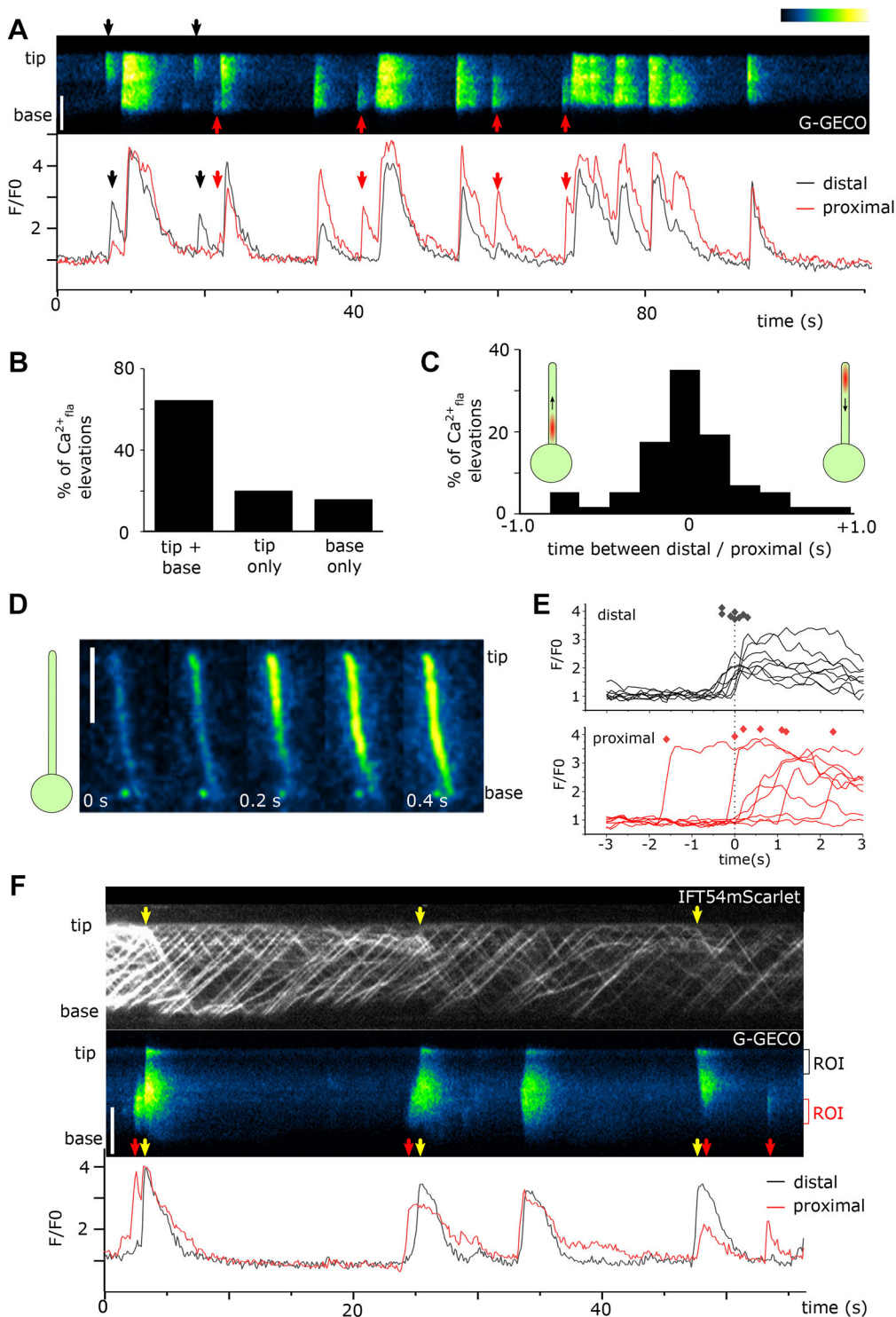


Fig. 8. $[\text{Ca}^{2+}]_{\text{fla}}$ elevations have distinct spatial properties.

(A) Localised Ca^{2+} elevations in either the distal (black arrow) or proximal (red arrow) region of the flagellum. Scale bar: 5 μm . (B) The percentage of $[\text{Ca}^{2+}]_{\text{fla}}$ elevations that occur across the whole flagellum or are restricted to distal or proximal regions. $n=250$ $[\text{Ca}^{2+}]_{\text{fla}}$ elevations from seven flagella. (C) Time difference between the rise time of $[\text{Ca}^{2+}]_{\text{fla}}$ elevations in the distal region compared to proximal region (see diagram). Positive numbers for $[\text{Ca}^{2+}]_{\text{fla}}$ elevations that initiate in the distal region. $n=57$ elevations from nine flagella. Bin size, 0.2 s. (D) A typical $[\text{Ca}^{2+}]_{\text{fla}}$ elevation propagating from the distal region. Diagram on left shows position of flagellum relative to the cell body. Scale bar: 5 μm . (E) Timing of $[\text{Ca}^{2+}]_{\text{fla}}$ elevations in the distal and proximal regions of the flagellum (diamonds), displayed relative to the movement of paused retrograde IFT trains in the distal region (dotted line). $[\text{Ca}^{2+}]_{\text{fla}}$ elevations in the distal region coincide with the movement of IFT trains. (F) Simultaneous imaging of $[\text{Ca}^{2+}]_{\text{fla}}$ and IFT54-mScarlet indicates that movement of paused retrograde IFT trains in the distal region of the flagellum (yellow arrows) coincides with colocalising $[\text{Ca}^{2+}]_{\text{fla}}$ elevations in the proximal region. Red arrows indicate the timing of $[\text{Ca}^{2+}]_{\text{fla}}$ elevations in the proximal region. Scale bar: 5 μm .

flagella detachment. *Chlamydomonas* cells suspended on a micropipette lift their flagella from a surface within 30 s after removing blue light (Kreis et al., 2018). We found that removing blue light illumination from adherent IFT54-MS cells also promoted flagella detachment, with 11 out of 14 flagella lifting from the surface entirely or remaining only attached at the flagella tips within 30 s (Fig. S6D). Flagella movements prior to lifting were preceded by the removal of paused retrograde IFT trains (Fig. S6E). Note that it was not possible to measure $[\text{Ca}^{2+}]_{\text{fla}}$ directly while using blue light to

modulate adhesion, as G-GECO requires excitation with blue light. However, removing blue light illumination in the absence of external Ca^{2+} did not lead to flagella lifting (0 out of 17 cells) and paused retrograde IFT trains remained in the distal regions (Fig. S6F). The removal of external Ca^{2+} did not act to simply immobilise flagella, as non-adherent cells continued to actively swim in this period. Together, the results suggest that light-dependent detachment of flagella from a surface requires the Ca^{2+} -dependent release of flagella membrane glycoproteins from paused retrograde IFT trains.

DISCUSSION

Our results help to provide a mechanistic understanding of the requirement for Ca^{2+} in flagella surface motility and gliding in *Chlamydomonas*. We previously demonstrated that $[\text{Ca}^{2+}]_{\text{fla}}$ elevations are linked to the movement of paused retrograde IFT trains (Collingridge et al., 2013), although alternative roles for Ca^{2+} in promoting the pausing of retrograde IFT have also been proposed (Shih et al., 2013). By using improved techniques to visualise $[\text{Ca}^{2+}]_{\text{fla}}$ elevations in *Chlamydomonas*, our results demonstrate that $[\text{Ca}^{2+}]_{\text{fla}}$ elevations act to initiate the movement of paused retrograde IFT trains by disrupting an interaction between the IFT particle and flagella membrane glycoproteins. By regulating the accumulation of paused retrograde IFT motors, this process modulates the generation of motive force in individual adherent flagella. We did not find evidence for a requirement for $[\text{Ca}^{2+}]_{\text{fla}}$ elevations in regulating other aspects of IFT, for example, by promoting the pausing of anterograde and/or retrograde IFT trains or influencing their velocity. Chien et al. (2017) found that the removal of external Ca^{2+} increased the residency of IFT trains at the flagella tip, suggesting that Ca^{2+} may also have a regulatory role in the assembly or departure of retrograde trains. We were not able to directly assess the turnaround of IFT trains in our analyses. However, our experiments show that retrograde IFT trains continue to accumulate in the absence of external Ca^{2+} , indicating that IFT turnaround continues in the absence of $[\text{Ca}^{2+}]_{\text{fla}}$ elevations.

These findings allow us to further develop the proposed model for gliding motility in *Chlamydomonas* (Bloodgood, 2009; Collingridge et al., 2013; Shih et al., 2013) (Fig. S7). When a cell first encounters a solid surface, often only the distal regions of the flagella adhere to the surface. Both flagella subsequently glide forward, which brings the entire length of each flagellum into contact with the surface. The gliding movement is driven by retrograde IFT motors engaging with FMG-1B in the flagella membrane, which adheres to the surface (Shih et al., 2013). Once the flagella become fully extended in the gliding configuration, the two flagella are arranged at 180° to each other and are pulling in opposite directions. If the traction forces generated by each flagella are balanced, neither flagellum can move forward and there is no net movement of the cell. The traction forces increase as further retrograde IFT trains engage with FMG-1B in each flagellum. When the membrane tension reaches a critical threshold in one flagellum, a Ca^{2+} elevation is generated, which disrupts the interaction between the retrograde IFT trains and FMG-1B, selectively disrupting the traction force in this flagellum. The trailing flagellum therefore no longer resists the force generated by the opposing flagellum (the leading flagellum), which is able to pull the cell forward along the surface.

The Ca^{2+} -dependent regulation of the interactions between IFT and the flagella membrane should also be considered in the context of flagella adhesion. As flagella lifting requires the flagellum to be pulled towards the cell body, modulation of the traction force generated by each flagellum will influence its ability to resist this pulling force. When retrograde IFT trains engage with FMG-1B, they act to resist movement of the flagellum in the direction of the cell body. However, when not in contact with anterograde or retrograde IFT trains, FMG-1B can diffuse freely along the flagellum, as demonstrated by microsphere movements (Bloodgood et al., 2019). This allows an adherent flagellum to slide along a surface while maintaining contact with the surface. During this movement, some of the FMG-1B is shed onto the surface (Kamiya et al., 2018) (Fig. S8). As $[\text{Ca}^{2+}]_{\text{fla}}$ elevations act to disengage FMG-1B from retrograde IFT trains, they allow unrestricted movement of FMG-1B along the membrane. $[\text{Ca}^{2+}]_{\text{fla}}$

elevations therefore do not modify adhesion directly, but influence the ability of flagella to resist a pulling force.

$[\text{Ca}^{2+}]_{\text{fla}}$ elevations on an untreated surface are primarily observed in flagella under tension, i.e. immediately prior to trailing or lifting movements. By disrupting the interaction between IFT and the flagella membrane, the $[\text{Ca}^{2+}]_{\text{fla}}$ elevations act to reduce the membrane tension. On a highly adherent surface, $[\text{Ca}^{2+}]_{\text{fla}}$ elevations are observed in the absence of movement, suggesting that flagella immobilisation itself causes membrane tension. Although the repetitive $[\text{Ca}^{2+}]_{\text{fla}}$ elevations act to prevent the accumulation of retrograde IFT trains, in this situation the membrane tension is not relieved and the flagella remain immobilised due to the highly adherent nature of the surface.

The proposed model for gliding motility illustrates how the cell is able to coordinate interactions between retrograde IFT motors and flagella membrane glycoproteins in order to modulate the traction force in individual flagella while they are adhered to a surface. However, some important questions remain regarding the underlying molecular mechanisms. How does $[\text{Ca}^{2+}]_{\text{fla}}$ act to disrupt the interaction between IFT and FMG-1B? How is the $[\text{Ca}^{2+}]_{\text{fla}}$ elevation generated in a single flagellum? What mechanisms enable the generation of repetitive $[\text{Ca}^{2+}]_{\text{fla}}$ elevations? These questions represent important avenues for future investigation.

The interaction between the IFT particle and FMG-1B is implied from the coordinated movement of fluorescent microspheres and IFT trains (Shih et al., 2013), but biochemical characterisation of this interaction is lacking. Recent characterisation of an *fmg-1b* mutant line (Bloodgood et al., 2019) supports previous observations that FMG-1B is the primary protein in the flagellum mediating contact with solid substrates (Bloodgood, 1982, 1984), although an additional flagella membrane glycoprotein, FAP113, was recently identified as interacting with microspheres (Kamiya et al., 2018). It seems likely that surface contact, which induces cross-linking of FMG-1B (Bloodgood and Salomonsky, 1998), acts to promote an interaction between FMG-1B and retrograde IFT trains, as retrograde IFT trains do not accumulate in non-adherent flagella (Collingridge et al., 2013). We propose that the increase in $[\text{Ca}^{2+}]_{\text{fla}}$ likely leads to a direct conformational shift in a Ca^{2+} -sensitive protein within the putative IFT–FMG-1B complex, disrupting the interaction. This mechanism would be analogous to the Ca^{2+} -regulated movement of mitochondria along microtubules in neurons and other animal cell types, where the interaction between the mitochondrion and kinesin or dynein is mediated by the Ca^{2+} -binding Rho-GTPase Miro (Saotome et al., 2008). Elevated cytosolic Ca^{2+} triggers a conformational change in Miro, which possesses two Ca^{2+} -binding EF-hands, leading to the dissociation of the mitochondrion from the microtubule motor complex (Wang and Schwarz, 2009). $[\text{Ca}^{2+}]_{\text{fla}}$ elevations in adherent flagella are most likely initiated by the activation of mechanosensitive ion channels in the flagella membrane. *Chlamydomonas* flagella contain a number of candidate ion channels that may contribute to signalling in response to changes in membrane tension (Bezares-Calderon et al., 2020; Wheeler, 2017; Yoshimura, 1996). The transient receptor potential (TRP) channel TRP11 is required for the mechanosensitive response of swimming *Chlamydomonas* cells (Fujiu et al., 2011). *Chlamydomonas* flagella also possess a homologue of polycystin-2 (PKD2), which has been implicated in mechanosensation in mammalian cilia, although direct evidence for mechanosensory Ca^{2+} signalling in primary cilia is lacking (Delling et al., 2016; Lee et al., 2015). *Chlamydomonas* PKD2 localises to the flagella membrane, but is also bound to the axoneme and to extracellular glycoprotein polymers known as mastigonemes, which

resemble hair-like appendages along the distal regions of the flagella (Huang et al., 2007; Liu et al., 2020). The tethering of PKD2 to mastigonemes and the axoneme supports a mechanosensory role for this ion channel in *Chlamydomonas* (Liu et al., 2020).

Although mechanosensitive ion channels may contribute to $[Ca^{2+}]_{fla}$ elevations directly, the permeation of cations through these channels will also act to depolarise the flagella membrane, which may activate voltage-gated Ca^{2+} channels along the length of the flagellum. The presence of voltage-gated Ca^{2+} channels in *Chlamydomonas* flagella is well documented (Fujiu et al., 2009; Holland et al., 1996), and we have previously observed transient depolarisations in the flagella membrane during gliding motility (Collingridge et al., 2013). If the stimulus (i.e. membrane tension) persists, the voltage-gated Ca^{2+} channels can activate again following a refractory period, leading to a series of repetitive Ca^{2+} elevations. Increasing membrane tension could shorten this refractory period, increasing the frequency of the $[Ca^{2+}]_{fla}$ elevations. Repetitive Ca^{2+} elevations generated by the activity of voltage-gated Ca^{2+} channels can be observed in many excitable cell types, including sperm flagella, in the continued presence of a stimulus (Kaupp et al., 2008; Kotov et al., 2011).

The presence of localised or propagating $[Ca^{2+}]_{fla}$ elevations suggests that flagella Ca^{2+} signalling may also exhibit greater complexity. It is possible that the propagating $[Ca^{2+}]_{fla}$ elevations represent simple diffusion of Ca^{2+} in the flagella matrix following a localised $[Ca^{2+}]_{fla}$ elevation. Ca^{2+} elevations initiating in the cytosol can diffuse along the cilia of mammalian ependymal cells at a rate of $\sim 20 \mu m s^{-1}$ (Doerner et al., 2015). However, cytosolic Ca^{2+} elevations are not directly coupled to $[Ca^{2+}]_{fla}$ elevations in *Chlamydomonas* (Bickerton et al., 2016). Moreover, *Chlamydomonas* flagella possess ion channels typically associated with propagating Ca^{2+} elevations in animal cells. Inositol triphosphate receptors (IP₃Rs) typically localise to endomembranes in mammalian cells, where they contribute to fast cytosolic Ca^{2+} waves through Ca^{2+} -activated Ca^{2+} release. A homologue of mammalian IP₃Rs is present in *Chlamydomonas* flagella (Pazour et al., 2005), which could potentially mediate propagation of localised $[Ca^{2+}]_{fla}$ elevations through Ca^{2+} -activated Ca^{2+} influx.

The development of flagella-localised Ca^{2+} -reporters in *Chlamydomonas* should aid the identification of ion channels responsible for Ca^{2+} signalling in adherent flagella. However, the nature of flagella adhesion and membrane tension will be a critical consideration for future studies of flagella Ca^{2+} signalling, particularly when comparing phenotypes between strains. Gliding motility is often markedly different between strains and rapid light-dependent modulation of flagella adhesion can occur within seconds in individual cells (Kreis et al., 2018). The lack of mastigonemes in *pkd2* mutants indicates that loss of ion channel function may also influence the arrangement of flagella glycoproteins (Liu et al., 2020). Although mastigonemes are not thought to be involved in microsphere movements or gliding motility in *Chlamydomonas* (Bloodgood, 1977; Nakamura et al., 1996), they have been implicated in flagella-dependent gliding motility in *Peranema* (Saito et al., 2003). Thus, knockout of an ion channel could influence the processes that trigger $[Ca^{2+}]_{fla}$ elevations (i.e. flagella adhesion), as well as the signalling processes themselves. Without direct measurements of the degree of adhesion and/or membrane tension in these mutant strains, it may be difficult to ascertain whether any effects on Ca^{2+} signalling result from direct mechanistic inhibition of $[Ca^{2+}]_{fla}$ elevations or relate to indirect effects on flagella adhesion.

It is becoming clear that the nature of ciliary Ca^{2+} signalling differs markedly between organisms and cell types (Pablo et al., 2017). Rapid changes in flagella Ca^{2+} have a well-characterised role in the swimming motility of *Chlamydomonas*, in addition to their role in gliding motility (Holland et al., 1997). Ca^{2+} -dependent signalling mechanisms also regulate swimming of ciliates such as *Paramecium* (Eckert and Brehm, 1979) and metazoan sperm (Kaupp et al., 2008). While it is likely that flagella-localised voltage-gated Ca^{2+} channels contribute directly to $[Ca^{2+}]_{fla}$ elevations in *Chlamydomonas* and *Paramecium* (Eckert and Brehm, 1979; Fujiu et al., 2009), their role in mammalian sperm flagella are less clear, where the weakly-voltage-gated CatSper channels are primary contributors to flagella Ca^{2+} elevations (Lishko et al., 2012). Although CatSper are also found in some protist lineages (e.g. glaucophytes), they are absent from *Chlamydomonas* (Cai et al., 2014). Furthermore, although voltage-gated Ca^{2+} channels are present in motile ependymal cilia of mammalian cells, ciliary Ca^{2+} in these cells appears to be passively coupled to $[Ca^{2+}]_{cyt}$ rather than being independently controlled (Doerner et al., 2015). The nature of Ca^{2+} signalling in the non-motile primary cilia of mammalian cells is also highly distinct from the excitable cilia of unicellular protists (Delling et al., 2013). Therefore, although Ca^{2+} -dependent signalling mechanisms appear to be ubiquitous in cilia and flagella, the nature of these mechanisms and their underlying molecular components differ considerably between eukaryotes.

Interactions between IFT complexes and their cargo proteins underpin many aspects of ciliary function (Bhogaraju et al., 2013b). Our results indicate that Ca^{2+} plays an important regulatory role in the interactions between IFT trains and flagella membrane glycoproteins in *Chlamydomonas*. As FMG-1B is a highly abundant protein in *Chlamydomonas* flagella, these transient interactions can be detected through the movement of microspheres or during gliding motility. However, it is likely that similar regulatory mechanisms direct the movement of many other flagella membrane proteins. Future biochemical characterisation of the FMG-1B-IFT complex, and in particular the identification of the Ca^{2+} -sensitive components that mediate the response to $[Ca^{2+}]_{fla}$ elevations, will help identify whether these mechanisms are conserved in other ciliated organisms.

MATERIALS AND METHODS

Strains and culture conditions

Chlamydomonas reinhardtii cells were grown in standard Tris-acetate-phosphate (TAP) medium at 21°C on a 16 h light–8 h dark cycle with a photosynthetic photon flux density of $80 \mu mol m^{-2} s^{-1}$. Wild-type strains CC-125 and CC-5325 and the IFT reporter strains D1bLIC-GFP (CC-4488) (Reck et al., 2016) and KAP-GFP [CC-4296 - *fla3-1* background (Mueller et al., 2005)] strain were obtained from the *Chlamydomonas* Resource Centre (<http://chlamycollection.org/>). *Chlamydomonas* strains expressing CAH6-Venus and IFT27-GFP (CC-125 background) were obtained from Luke Mackinder (University of York, UK) and Joel Rosenbaum (Yale University, CT), respectively (Mackinder et al., 2017; Qin et al., 2007). IFT20-mCherry [null *ift20* background (Lechtreck et al., 2009)] and the IFT54-mScarlet reporter strain (IFT54-MS) were provided by Karl Lechtreck (University of Georgia, Atlanta, GA). The IFT54-MS strain was constructed by expressing IFT54-mScarlet in an *ift54-2* background (Wingfield et al., 2017). The IFT54-mScarlet vector was made by cutting out mNeonGreen from pBR25-mNG-IFT54 using *XhoI* and *BamHI* and replaced with a PCR product encoding IFT54-mScarlet using the mammalian codon usage trimmed with the same enzymes (Wingfield et al., 2017).

Development of a flagella-targeted Ca^{2+} sensor

The flagella-targeted Ca^{2+} reporter was prepared by modifying the pLM005-CAH6-Venus vector (obtained from Luke Mackinder, University of York, UK) used to express the flagella-localised carbonic

anhydrase CAH6 (Mackinder et al., 2017). Codon-optimised G-GECO1.1 was synthesised (Genscript) and introduced into the pLM005-CAH6-Venus expression vector via the sites *BglIII* and *EcoRI*, resulting in a C-terminal fusion of G-GECO to CAH6, separated by a short amino acid linker sequence. The GG-WT and GG-IFT54-MS strains were produced by transforming *C. reinhardtii* strains CC-5325 (wild type) and IFT54-MS by electroporation using a NEPA21 Super Electroporator (NepaGene, Japan) (Yamano et al., 2013). Cells were grown to a cell density of 1×10^7 – 2×10^7 cells ml^{-1} . The cultured cells were collected by centrifugation (400 g, 3 min) and re-suspended in TAP media containing 40 mM sucrose to a final density of 1×10^8 – 1.5×10^8 cells ml^{-1} . 1×10^7 cells and 350 ng of plasmid DNA (pLM005-CAH6-G-GECO construct linearized with *EcoRI*) were suspended in a total volume of 20–30 μl and placed into an electroporation cuvette (2 mm). The measured value of electric impedance was within 500–650 Ω . Electroporation utilised a first pulse (Pp) at 250 V with 8 ms pulse length, 50 ms pulse interval and 40% decay rates. The second pulse consisted of multiple transfer pulses (Tp) of 20 V with 50 ms pulse length, 50 ms pulse interval and 40% decay rate (two iterations). Cells were transferred into 10 ml TAP medium containing 40 mM sucrose and incubated in dim light (2 – $3 \mu\text{mol photons m}^{-2} \text{s}^{-1}$) for 24 h. The cells were collected by centrifugation (400 g, 3 min) and plated onto 1.5% agar TAP plate containing 10 $\mu\text{g ml}^{-1}$ hygromycin B (Roche) and 20 $\mu\text{g ml}^{-1}$ of paromomycin sulfate (Fisher BioReagents).

Biolistic loading of Ca^{2+} dyes

For experiments where flagella Ca^{2+} was measured using fluorescent dyes, dyes were loaded into cells using a biolistic approach (Collingridge et al., 2013). For this, 0.9 mg of 0.6 μm diameter gold microcarriers (Bio-Rad) were coated in 40 μg Oregon Green–BAPTA–dextran (10,000 molecular mass) and 24 μg Texas Red–dextran (10,000 molecular mass) (Invitrogen). Oregon Green–BAPTA is Ca^{2+} -responsive, whereas Texas Red acts as a non-responsive reference dye. Texas Red was omitted for simultaneous imaging of Ca^{2+} and IFT20–mCherry. *Chlamydomonas* cells (strain CC-125) were harvested in mid-exponential phase by gentle centrifugation (400 g for 3 min) and resuspended in loading buffer (10 mM HEPES pH 7.4, 20 μM K^+ glutamate and 50 mM sorbitol). Then, 5×10^6 cells were spread onto a 0.45 μm nitrocellulose membrane filter (Millipore) and loaded biolistically using a PDS-1000 delivery system (Bio-Rad) (1100 psi rupture disc). After loading, cells were washed and resuspended in TAP medium and allowed to recover for at least 2 h prior to imaging.

TIRF imaging of flagella

For all experiments, *Chlamydomonas* cells were suspended in a HEPES/NMG buffer consisting of 5 mM HEPES, 1 mM KCl, 1 mM HCl, 500 μM CaCl_2 , 200 μM EGTA (free Ca^{2+} 301 μM) and pH adjusted to 7.4 with N-methyl-D-glucamine (Holland et al., 1997). To remove external Ca^{2+} , cells were perfused with a Ca^{2+} -free buffer in which CaCl_2 had been omitted. Cells were added to 35 mm glass bottom dishes (In Vitro Scientific), which in some cases were treated with 0.1% poly-L-lysine to promote flagella adhesion. TIRF microscopy was performed at room-temperature using a Nikon Eclipse Ti with 100 \times (1.49 NA) TIRF oil immersion objective and an EM-CCD camera (Photometrics Evolve). TIRF was achieved via through-the-lens laser illumination. Wavelength compensation was not applied. IFT20–mCherry and IFT54–mScarlet were excited using a 561 nm laser (Coherent), with emission at 575–625 nm. IFT27–GFP, Venus and G-GECO were excited using a 488 nm laser (Coherent), with emission at 500–550 nm. For two-channel imaging, simultaneous TIRF excitation was performed at 488 and 561 nm and a dual-view beam-splitter device was used to detect emission at 505–535 and 605–655 nm. Images were captured using NIS-Elements software (v3.1) at 100 ms per frame unless otherwise stated. Imaging of OGB was at 300 ms per frame. We found that dual channel imaging of G-GECO and IFT54–mScarlet led to some photobleaching of mScarlet in paused IFT trains, unless laser emission intensities were reduced. Therefore, to quantify the accumulation of paused IFT trains (Fig. 6; Fig. S4) we used Oregon Green–BAPTA in the IFT20–mCherry reporter strain, as photobleaching of paused IFT trains was not observed in these imaging conditions.

Fluorescence emission from single wavelength indicators, such as G-GECO, can be influenced by imaging artefacts such as flagella movement in the TIRF field of illumination. The use of a single emission wavelength Ca^{2+} indicator was necessary for simultaneous imaging of IFT processes. We therefore performed a series of validation experiments to confirm that G-GECO was a reliable reporter of flagella Ca^{2+} elevations as follows: (1) Rapid transient elevations in G-GECO fluorescence were not seen in the absence of external Ca^{2+} (Fig. 3D). (2) G-GECO has a high dynamic range, exhibiting large changes in fluorescence emission on Ca^{2+} binding. Similar elevations in fluorescence were never observed in cells expressing CAH6–Venus, even during gliding motility (Fig. S2), indicating that motion artefacts do not give rise to large increases in fluorescence. (3) The nature of the $[\text{Ca}^{2+}]_{\text{fla}}$ elevations (e.g. duration, frequency) observed using G-GECO were very similar to those observed using ratiometric imaging of the fluorescent dyes OGB and Texas Red–Dextran (Collingridge et al., 2013). Key findings using G-GECO were also verified using OGB (e.g. Fig. S3). (4) For detailed examination of $[\text{Ca}^{2+}]_{\text{fla}}$ and IFT, imaging of G-GECO was performed primarily in flagella immobilised with 0.1% poly-L-lysine to ensure that motion artefacts were minimised. (5) Dual-channel imaging of G-GECO and IFT54–mScarlet enabled visual confirmation that changes in the intensity of G-GECO fluorescence were not replicated in the IFT54–mScarlet channel and were therefore due to changes in $[\text{Ca}^{2+}]_{\text{fla}}$ (Fig. S6C). This was particularly important for confirming that localised $[\text{Ca}^{2+}]_{\text{fla}}$ elevations were not artefacts due to flagella movement (e.g. Fig. 7A).

Red fluorescent carboxylate-modified microspheres (0.1 μm diameter, Thermo Fisher) were used to image flagellar surface motility. Microspheres diluted in HEPES/NMG buffer were added to adherent cells and imaged by TIRF microscopy. Excitation with a 488 nm laser alone was sufficient to simultaneously image G-GECO and microspheres due to the very high fluorescence emission of the microspheres. A dual-view beam-splitter device was used to detect emission at 505–535 nm (G-GECO or IFT27–GFP) and 605–655 nm (microspheres). Flagella exhibiting microsphere movements greater than 1 μm were examined for the presence of $[\text{Ca}^{2+}]_{\text{fla}}$ elevations during the course of microsphere movement.

For modulation of flagella adhesion with blue light, IFT54-MS cells were imaged by TIRF microscopy as described above, but a 488 nm laser was used to provide stimulation with blue light. Blue light was applied for 2 min to allow flagella to attach to the glass surface and then flagella lifting was examined after removing blue light for 30 s (defined as the removal of flagella from the surface, or a >50% decrease in flagella area in contact with the surface).

For imaging of flagella membrane glycoproteins, cells were stained with the fluorescent lectin concanavalin A (ConA) (100 $\mu\text{g ml}^{-1}$) conjugated to fluorescein isothiocyanate (FITC) (Invitrogen, UK) for 5 min. Cells were then centrifuged (400 g, 1 min) and resuspended in HEPES/NMG buffer prior to TIRF imaging.

Data processing

Images were smoothed using a 3 \times 3 pixel filter (NIS elements) and kymographs were generated using ImageJ software (version 1.45 s; <http://rsb.info.nih.gov/ij/>). To identify $[\text{Ca}^{2+}]_{\text{fla}}$ elevations, we calculated the mean pixel intensity of G-GECO within a region of interest encompassing the whole flagellum, unless stated otherwise. Distal and proximal regions of interest were defined as regions 1 μm in length at either end of the flagellum. For quantitative analysis, the baseline intensity was calculated using an asymmetric least squares smoothing algorithm (Origin Pro software, Northampton, MA) and changes in fluorescence emission were calculated using the ratio of fluorescence to the calculated baseline. Peaks were detected using Origin Pro software (peak finding method, local maximum with five local points), using a threshold value that differed from the baseline by 20%. IFT was monitored using TIRF microscopy of fluorescently tagged IFT proteins. A kymograph of 60 s duration was used to determine the mean velocity of IFT particles and the frequency at which they were observed within this time period. Entry of anterograde IFT trains was defined as the time at which the IFT train was first detected, as the region of the flagellum closest to the cell body may not be illuminated by TIRF excitation. IFT train velocity and frequency were quantified from the kymographs by measuring

the slope and number of traces, respectively using ICY software (de Chaumont et al., 2012). The interaction between IFT events and $[Ca^{2+}]_{fla}$ was examined by measuring relative G-GECO fluorescence coinciding with each event. To identify IFT events coinciding with the onset of $[Ca^{2+}]_{fla}$ elevations, a derivative Ca^{2+} trace was calculated by dividing the fluorescence in each frame by the median of the three preceding frames. The onset of each $[Ca^{2+}]_{fla}$ elevation was defined as the frame which displayed the greatest rate of change in fluorescence, and coinciding IFT events were defined as those events occurring within 0.5 s of this rise.

All statistical analyses were performed in Origin Pro Software (Northampton, MA). For the box plots, the box indicates the 25–75th percentiles with median, mean is the open square and whiskers represent 10–90th percentiles.

Fluorescence recovery after photobleaching

For FRAP analysis of IFT, IFT54-MS cells were observed with a Nikon Eclipse Ti E inverted fluorescence microscope, equipped with a dual View DV2 (Photometrics) to detect emission at 505–535 nm and 605–655 nm, a iLAS FRAP module (Roper Scientifics) and Hamamatsu Flash 04 LT camera. Images were acquired using Metamorph software (version 7.7, Molecular Devices). IFT54-MS cells were placed in a poly-L-lysine (0.01%) treated dish and kept at room temperature during the acquisition. A segment of a flagellum was bleached by irradiation with a 150 mW green laser (Vortran), delivered through the 100× TIRF oil objective lens (100×, APO TIRF oil immersion, NA 1.49, Nikon) used for observation and focused on the specimen. The position to be photobleached was set at 50–70% of the flagellar length from the tip. The intensity of laser beam was 30%. Laser light for photobleaching was usually irradiated for about 1 s. Images were recorded continuously for 15 s before bleaching and then recovery was monitored for 45 s by continuously recording videos with a 100 ms exposure.

Transmission electron microscopy

For chemical fixation of adherent *Chlamydomonas* flagella, cells were allowed to settle directly onto 0.01% poly-L-lysine-coated coverslips for 5 min. Excess cells were removed and cells were fixed with 1% glutaraldehyde in 0.1 M sodium cacodylate (pH 7.2) buffer for 10 min. Coverslips were washed three times for 5 min each in 0.1 M cacodylate buffer and then stained with 1% uranyl acetate in distilled water for 1 h at 4°C. Coverslips were washed three times for 10 min each in distilled water. After serial dehydration with ethanol solution (30%, 50%, 70%, 90% and three times at 100%), samples were embedded in Agar 100 resin (Agar Scientific). Coverslips were mounted in Agar 100 capsule and left to polymerize at 60°C for 2 days. To detach the coverslip, the sample was plunged into liquid nitrogen. First 200 nm ultrathin sections (50–70 nm) were collected in nickel grids Leica EM UC 7 Ultramicrotome and stained with uranyl acetate (1%) and lead citrate (80 mM). Observations were made on a Jeol 1400 TEM electron microscope. Images were processed with ImageJ.

Acknowledgements

We thank Karl Lehtreck (Georgia), Joel Rosenbaum (Yale) and Luke Mackinder (York) for the supply of *Chlamydomonas* strains. We thank Glenn Harper and Peter Bond from the Plymouth Electron Microscopy Centre (Plymouth University, UK) for assistance in the preparation of electron micrographs.

Competing interests

The authors declare no competing or financial interests.

Author contributions

Conceptualization: C.F., G.L.W.; Methodology: C.F., P.C., G.L.W.; Investigation: C.F., P.C., G.L.W.; Writing - original draft: G.L.W.; Writing - review & editing: C.F., C.B., G.L.W.; Visualization: G.L.W.; Supervision: C.B., G.L.W.; Project administration: C.B., G.L.W.; Funding acquisition: C.B., G.L.W.

Funding

The work was supported by a Biotechnology and Biological Sciences Research Council award to G.W. (BB/M02508X/1) and a European Research Council Advanced Grant to C.B. (ERC-ADG-670390).

Supplementary information

Supplementary information available online at <https://jcs.biologists.org/lookup/doi/10.1242/jcs.253492.supplemental>

Peer review history

The peer review history is available online at <https://jcs.biologists.org/lookup/doi/10.1242/jcs.253492.viewer-comments.pdf>

References

- Bezares-Calderón, L. A., Berger, J. and Jékely, G. (2020). Diversity of cilia-based mechanosensory systems and their functions in marine animal behaviour. *Philos. Trans. R. Soc. B Biol. Sci.* **375**, 20190376. doi:10.1098/rstb.2019.0376
- Bhogaraju, S., Cajanek, L., Fort, C., Blisnick, T., Weber, K., Taschner, M., Mizuno, N., Lamla, S., Bastin, P., Nigg, E. A. et al. (2013a). Molecular basis of tubulin transport within the cilium by IFT74 and IFT81. *Science* **341**, 1009–1012. doi:10.1126/science.1240985
- Bhogaraju, S., Engel, B. D. and Lorentzen, E. (2013b). Intraflagellar transport complex structure and cargo interactions. *Cilia* **2**, 10. doi:10.1186/2046-2530-2-10
- Bickerton, P., Sello, S., Brownlee, C., Pittman, J. K. and Wheeler, G. L. (2016). Spatial and temporal specificity of Ca^{2+} signalling in *Chlamydomonas reinhardtii* in response to osmotic stress. *New Phytol.* **212**, 920–933. doi:10.1111/nph.14128
- Bloodgood, R. A. (1977). Motility occurring in association with the surface of the *Chlamydomonas* flagellum. *J. Cell Biol.* **75**, 983–989. doi:10.1083/jcb.75.3.983
- Bloodgood, R. A. (1981). Flagella-dependent gliding motility in *Chlamydomonas*. *Protoplasma* **106**, 183–192. doi:10.1007/BF01275550
- Bloodgood, R. A. (1982). Dynamic properties of the flagellar surface. *Symp. Soc. Exp. Biol.* **35**, 353–380.
- Bloodgood, R. A. (1984). Preferential turnover of membrane proteins in the intact *Chlamydomonas* flagellum. *Exp. Cell Res.* **150**, 488–493. doi:10.1016/0014-4827(84)90594-9
- Bloodgood, R. A. (1995). Flagellar surface motility: gliding and microsphere movements. *Methods Cell Biol.* **47**, 273–279. doi:10.1016/S0091-679X(08)60820-1
- Bloodgood, R. A. (2009). The *Chlamydomonas* flagellar membrane and its dynamic properties. In *The Chlamydomonas Sourcebook* (ed. G.B. Witman), pp. 309–368. Oxford: Academic Press.
- Bloodgood, R. A. and Salomonsky, N. L. (1990). Calcium influx regulates antibody-induced glycoprotein movements within the *Chlamydomonas* flagellar membrane. *J. Cell Sci.* **96**, 27–33.
- Bloodgood, R. A. and Salomonsky, N. L. (1998). Microsphere attachment induces glycoprotein redistribution and transmembrane signaling in the *Chlamydomonas* flagellum. *Protoplasma* **202**, 76–83. doi:10.1007/BF01280876
- Bloodgood, R. A. and Workman, L. J. (1984). A flagellar surface glycoprotein mediating cell-substrate interaction in *Chlamydomonas*. *Cell Motil.* **4**, 77–87. doi:10.1002/cm.970040202
- Bloodgood, R. A., Tetreault, J. and Sloboda, R. D. (2019). The *Chlamydomonas* flagellar membrane glycoprotein FMG-1B is necessary for expression of force at the flagellar surface. *J. Cell Sci.* **132**, jcs233429. doi:10.1242/jcs.233429
- Cai, X., Wang, X. and Clapham, D. E. (2014). Early evolution of the eukaryotic Ca^{2+} signaling machinery: conservation of the CatSper channel complex. *Mol. Biol. Evol.* **31**, 2735–2740. doi:10.1093/molbev/msu218
- Chien, A., Shih, S. M., Bower, R., Tritschler, D., Porter, M. E. and Yildiz, A. (2017). Dynamics of the IFT machinery at the ciliary tip. *eLife* **6**, e28606. doi:10.7554/eLife.28606
- Collingridge, P., Brownlee, C. and Wheeler, G. L. (2013). Compartmentalized calcium signaling in cilia regulates intraflagellar transport. *Curr. Biol.* **23**, 2311–2318. doi:10.1016/j.cub.2013.09.059
- Dai, J., Barbieri, F., Mitchell, D. R. and Lehtreck, K. F. (2018). In vivo analysis of outer arm dynein transport reveals cargo-specific intraflagellar transport properties. *Mol. Cell* **29**, 2553–2565. doi:10.1091/mbc.E18-05-0291
- de Chaumont, F., Dallongeville, S., Chenouard, N., Hervé, N., Pop, S., Provoost, T., Meas-Yedid, V., Pankajakshan, P., Lecomte, T., Le Montagner, Y. et al. (2012). Icy: an open bioimage informatics platform for extended reproducible research. *Nat. Methods* **9**, 690–696. doi:10.1038/nmeth.2075
- Delling, M., DeCaen, P. G., Doerner, J. F., Febvay, S. and Clapham, D. E. (2013). Primary cilia are specialized calcium signalling organelles. *Nature* **504**, 311–314. doi:10.1038/nature12833
- Delling, M., Indzhukulian, A. A., Liu, X., Li, Y., Xie, T., Corey, D. P. and Clapham, D. E. (2016). Primary cilia are not calcium-responsive mechanosensors. *Nature* **531**, 656–660. doi:10.1038/nature17426
- Dentler, W., Vanderwaal, K. and Porter, M. E. (2009). Recording and analyzing IFT in *Chlamydomonas* flagella. *Methods Cell Biol.* **93**, 145–155. doi:10.1016/S0091-679X(08)93008-9
- Doerner, J. F., Delling, M. and Clapham, D. E. (2015). Ion channels and calcium signaling in motile cilia. *eLife* **4**, e11066. doi:10.7554/eLife.11066
- Eckert, R. and Brehm, P. (1979). Ionic mechanisms of excitation in *Paramecium*. *Annu. Rev. Biophys. Bioeng.* **8**, 353–383. doi:10.1146/annurev.bb.08.060179.002033
- Engel, B. D., Lehtreck, K. F., Sakai, T., Ikebe, M., Witman, G. B. and Marshall, W. F. (2009). Total internal reflection fluorescence (TIRF) microscopy of

- Chlamydomonas* flagella. *Methods Cell Biol.* **93**, 157-177. doi:10.1016/S0091-679X(08)93009-0
- Engel, B. D., Ishikawa, H., Wemmer, K. A., Geimer, S., Wakabayashi, K., Hirono, M., Craige, B., Pazour, G. J., Witman, G. B., Kamiya, R. et al. (2012). The role of retrograde intraflagellar transport in flagellar assembly, maintenance, and function. *J. Cell Biol.* **199**, 151-167. doi:10.1083/jcb.201206068
- Foreman, J., Demichchik, V., Bothwell, J. H. F., Mylona, P., Miedema, H., Torres, M. A., Linstead, P., Costa, S., Brownlee, C., Jones, J. D. G. et al. (2003). Reactive oxygen species produced by NADPH oxidase regulate plant cell growth. *Nature* **422**, 442-446. doi:10.1038/nature01485
- Fujiu, K., Nakayama, Y., Yanagisawa, A., Sokabe, M. and Yoshimura, K. (2009). *Chlamydomonas* CAV2 encodes a voltage-dependent calcium channel required for the flagellar waveform conversion. *Curr. Biol.* **19**, 133-139. doi:10.1016/j.cub.2008.11.068
- Fujiu, K., Nakayama, Y., Iida, H., Sokabe, M. and Yoshimura, K. (2011). Mechanoreception in motile flagella of *Chlamydomonas*. *Nat. Cell Biol.* **13**, 630-632. doi:10.1038/ncb2214
- Goodenough, U. W., Shames, B., Small, L., Saito, T., Crain, R. C., Sanders, M. A. and Salisbury, J. L. (1993). The role of calcium in the *Chlamydomonas reinhardtii* mating reaction. *J. Cell Biol.* **121**, 365-374. doi:10.1083/jcb.121.2.365
- Hegemann, P. and Berthold, P. (2009). Sensory photoreceptors and light control of flagellar activity. In *The Chlamydomonas Sourcebook* (ed. G.B. Witman), pp. 395-429. Oxford: Academic Press.
- Hendel, N. L., Thomson, M. and Marshall, W. F. (2018). Diffusion as a ruler: modeling kinesin diffusion as a length sensor for intraflagellar transport. *Biophys. J.* **114**, 663-674. doi:10.1016/j.bpj.2017.11.3784
- Holland, E.-M., Braun, F.-J., Nonnengässer, C., Harz, H. and Hegemann, P. (1996). The Nature of rhodopsin-triggered photocurrents in *Chlamydomonas*. I. Kinetics and influence of divalent ions. *Biophys. J.* **70**, 924-931. doi:10.1016/S0006-3495(96)79635-2
- Holland, E. M., Harz, H., Uhl, R. and Hegemann, P. (1997). Control of phobic behavioral responses by rhodopsin-induced photocurrents in *Chlamydomonas*. *Biophys. J.* **73**, 1395-1401. doi:10.1016/S0006-3495(97)78171-2
- Huang, K., Diener, D. R., Mitchell, A., Pazour, G. J., Witman, G. B. and Rosenbaum, J. L. (2007). Function and dynamics of PKD2 in *Chlamydomonas reinhardtii* flagella. *J. Cell Biol.* **179**, 501-514. doi:10.1083/jcb.200704069
- Kamiya, R., Shiba, K., Inaba, K. and Kato-Minoura, T. (2018). Release of sticky glycoproteins from *Chlamydomonas* flagella during microsphere translocation on the surface membrane. *Zoolog. Sci.* **35**, 299-305. doi:10.2108/zs180025
- Kaupp, U. B., Kashikar, N. D. and Weyand, I. (2008). Mechanisms of sperm chemotaxis. *Annu. Rev. Physiol.* **70**, 93-117. doi:10.1146/annurev.physiol.70.113006.100654
- Kotov, N. V., Bates, D. G., Gizatullina, A. N., Gilaziev, B., Khairullin, R. N., Chen, M. Z., Drozdov, I., Umezawa, Y., Hundhausen, C., Aleksandrov, A. et al. (2011). Computational modelling elucidates the mechanism of ciliary regulation in health and disease. *BMC Syst. Biol.* **5**, 143. doi:10.1186/1752-0509-5-143
- Kreis, C. T., Le Blay, M., Linne, C., Makowski, M. M. and Bäumchen, O. (2018). Adhesion of *Chlamydomonas* microalgae to surfaces is switchable by light. *Nat. Phys.* **14**, 45-49. doi:10.1038/nphys4258
- Kreis, C. T., Grangier, A. and Bäumchen, O. (2019). In vivo adhesion force measurements of *Chlamydomonas* on model substrates. *Soft Matter* **15**, 3027-3035. doi:10.1039/C8SM02236D
- Lechtreck, K. F. (2015). IFT-cargo interactions and protein transport in cilia. *Trends Biochem. Sci.* **40**, 765-778. doi:10.1016/j.tibs.2015.09.003
- Lechtreck, K. F., Johnson, E. C., Sakai, T., Cochran, D., Ballif, B. A., Rush, J., Pazour, G. J., Ikebe, M. and Witman, G. B. (2009). The *Chlamydomonas reinhardtii* BBSome is an IFT cargo required for export of specific signaling proteins from flagella. *J. Cell Biol.* **187**, 1117-1132. doi:10.1083/jcb.200909183
- Lee, K. L., Guevarra, M. D., Nguyen, A. M., Chua, M. C., Wang, Y. and Jacobs, C. R. (2015). The primary cilium functions as a mechanical and calcium signaling nexus. *Cilia* **4**, 7. doi:10.1186/s13630-015-0016-y
- Liang, Y., Pang, Y., Wu, Q., Hu, Z., Han, X., Xu, Y., Deng, H. and Pan, J. (2014). FLA8/KIF3B phosphorylation regulates kinesin-II interaction with IFT-B to control IFT entry and turnaround. *Dev. Cell* **30**, 585-597. doi:10.1016/j.devcel.2014.07.019
- Lishko, P. V., Kirichok, Y., Ren, D., Navarro, B., Chung, J.-J. and Clapham, D. E. (2012). The control of male fertility by spermatozoan ion channels. *Annu. Rev. Physiol.* **74**, 453-475. doi:10.1146/annurev-physiol-020911-153258
- Liu, P. and Lechtreck, K. F. (2018). The barbet-biedel syndrome protein complex is an adapter expanding the cargo range of intraflagellar transport trains for ciliary export. *Proc. Natl. Acad. Sci. USA* **115**, E934-E943. doi:10.1073/pnas.1713226115
- Liu, P., Lou, X., Wingfield, J. L., Lin, J., Nicastro, D. and Lechtreck, K. (2020). *Chlamydomonas* PKD2 organizes mastigonemes, hair-like glycoprotein polymers on cilia. *J. Cell Biol.* **219**, e202001122. doi:10.1083/jcb.202001122
- Mackinder, L. C. M., Chen, C., Leib, R. D., Patena, W., Blum, S. R., Rodman, M., Ramundo, S., Adams, C. M. and Jonikas, M. C. (2017). A spatial interactome reveals the protein organization of the algal CO₂-concentrating mechanism. *Cell* **171**, 133-147.e14. doi:10.1016/j.cell.2017.08.044
- Mueller, J., Perrone, C. A., Bower, R., Cole, D. G. and Porter, M. E. (2005). The FLA3 KAP subunit is required for localization of kinesin-2 to the site of flagellar assembly and processive anterograde intraflagellar transport. *Mol. Biol. Cell* **16**, 1341-1354. doi:10.1091/mbc.e04-10-0931
- Mukhopadhyay, S., Wen, X., Chih, B., Nelson, C. D., Lane, W. S., Scales, S. J. and Jackson, P. K. (2010). TULP3 bridges the IFT-A complex and membrane phosphoinositides to promote trafficking of G protein-coupled receptors into primary cilia. *Genes Dev.* **24**, 2180-2193. doi:10.1101/gad.1966210
- Mukhopadhyay, S., Wen, X., Ratti, N., Loktev, A., Rangell, L., Scales, S. J. and Jackson, P. K. (2013). The ciliary G-protein-coupled receptor Gpr161 negatively regulates the Sonic hedgehog pathway via cAMP signaling. *Cell* **152**, 210-223. doi:10.1016/j.cell.2012.12.026
- Nakamura, S., Tanaka, G., Maeda, T., Kamiya, R., Matsunaga, T. and Nikaido, O. (1996). Assembly and function of *Chlamydomonas* flagellar mastigonemes as probed with a monoclonal antibody. *J. Cell Sci.* **109**, 57-62.
- Pablo, J. L., DeCaen, P. G. and Clapham, D. E. (2017). Progress in ciliary ion channel physiology. *J. Gen. Physiol.* **149**, 37-47. doi:10.1085/jgp.201611696
- Pazour, G. J., Dickert, B. L. and Witman, G. B. (1999). The DHC1b (DHC2) isoform of cytoplasmic dynein is required for flagellar assembly. *J. Cell Biol.* **144**, 473-481. doi:10.1083/jcb.144.3.473
- Pazour, G. J., Agrin, N., Leszyk, J. and Witman, G. B. (2005). Proteomic analysis of a eukaryotic cilium. *J. Cell Biol.* **170**, 103-113. doi:10.1083/jcb.200504008
- Pedersen, L. B. and Rosenbaum, J. L. (2008). Intraflagellar transport (IFT): role in ciliary assembly, resorption and signalling. *Curr. Top. Dev. Biol.* **85**, 23-61. doi:10.1016/S0070-2153(08)00802-8
- Picariello, T., Brown, J. M., Hou, Y., Swank, G., Cochran, D. A., King, O. D., Lechtreck, K., Pazour, G. J. and Witman, G. B. (2019). A global analysis of IFT-A function reveals specialization for transport of membrane-associated proteins into cilia. *J. Cell Sci.* **132**, jcs220749. doi:10.1242/jcs.220749
- Qin, H., Wang, Z., Diener, D. and Rosenbaum, J. (2007). Intraflagellar transport protein 27 is a small G protein involved in cell-cycle control. *Curr. Biol.* **17**, 193-202. doi:10.1016/j.cub.2006.12.040
- Quarmby, L. M. (1996). Ca²⁺ influx activated by low pH in *Chlamydomonas*. *J. Gen. Physiol.* **108**, 351-361. doi:10.1085/jgp.108.4.351
- Reck, J., Schauer, A. M., VanderWaal Mills, K., Bower, R., Tritschler, D., Perrone, C. A. and Porter, M. E. (2016). The role of the dynein light intermediate chain in retrograde IFT and flagellar function in *Chlamydomonas*. *Mol. Biol. Cell* **27**, 2404-2422. doi:10.1091/mbc.e16-03-0191
- Saito, A., Suetomo, Y., Arikawa, M., Omura, G., Mostafa Kamal Khan, S. M., Kakuta, S., Suzuki, E., Kataoka, K. and Suzuki, T. (2003). Gliding movement in *Peranema trichophorum* is powered by flagellar surface motility. *Cell Motil. Cytoskeleton* **55**, 244-253. doi:10.1002/cm.10127
- Saotome, M., Saifulina, D., Szabadkai, G., Das, S., Fransson, A., Aspenstrom, P., Rizzuto, R. and Hajnoczky, G. (2008). Bidirectional Ca²⁺-dependent control of mitochondrial dynamics by the Miro GTPase. *Proc. Natl. Acad. Sci. USA* **105**, 20728-20733. doi:10.1073/pnas.0808953105
- Shih, S. M., Engel, B. D., Kocabas, F., Bilyard, T., Gennerich, A., Marshall, W. F. and Yildiz, A. (2013). Intraflagellar transport drives flagellar surface motility. *eLife* **2**, e00744. doi:10.7554/eLife.00744
- Steinhorst, L. and Kudla, J. (2013). Calcium - a central regulator of pollen germination and tube growth. *Biochim. Biophys. Acta (BBA) Mol. Cell Res.* **1833**, 1573-1581. doi:10.1016/j.bbamer.2012.10.009
- Stepanek, L. and Pigino, G. (2016). Microtubule doublets are double-track railways for intraflagellar transport trains. *Science* **352**, 721-724. doi:10.1126/science.aaf4594
- Wang, X. and Schwarz, T. L. (2009). The mechanism of Ca²⁺-dependent regulation of kinesin-mediated mitochondrial motility. *Cell* **136**, 163-174. doi:10.1016/j.cell.2008.11.046
- Wheeler, G. L. (2017). Calcium-dependent signalling processes in *Chlamydomonas*. In *Chlamydomonas: Molecular Genetics and Physiology* (ed. M. Hippler), pp. 233-255. Switzerland: Springer.
- Wingfield, J. L., Mengoni, I., Bomberger, H., Jiang, Y.-Y., Walsh, J. D., Brown, J. M., Picariello, T., Cochran, D. A., Zhu, B., Pan, J. et al. (2017). IFT trains in different stages of assembly queue at the ciliary base for consecutive release into the cilium. *eLife* **6**, e26609. doi:10.7554/eLife.26609
- Xu, N., Oltmanns, A., Zhao, L., Giroi, A., Karimi, M., Hoepfner, L., Kelterborn, S., Scholz, M., Beißel, J., Hegemann, P. et al. (2020). Altered N-glycan composition impacts flagella-mediated adhesion in *Chlamydomonas reinhardtii*. *eLife* **9**, e58805. doi:10.7554/eLife.58805
- Yamano, T., Iguchi, H. and Fukuzawa, H. (2013). Rapid transformation of *Chlamydomonas reinhardtii* without cell-wall removal. *J. Biosci. Bioeng.* **115**, 691-694. doi:10.1016/j.jbiosc.2012.12.020
- Yoshimura, K. (1996). A novel type of mechanoreception by the flagella of *Chlamydomonas*. *J. Exp. Biol.* **199**, 295-302.
- Yu, K., Liu, P., Venkatachalam, D., Hopkinson, B. M. and Lechtreck, K. F. (2020). The BBSome restricts entry of tagged carbonic anhydrase 6 into the cis-flagellum of *Chlamydomonas reinhardtii*. *PLoS ONE* **15**, e0240887. doi:10.1371/journal.pone.0240887